DISSERTATION

REEXAMINING THE ROLE OF LINKER HISTONES BEYOND 30 NM FIBERS IN A COMPLEX CHROMATIN ENVIRONMENT

Submitted by

Amanda Kuerzi

Department of Biochemistry and Molecular Biology

In partial fulfillment of the requirements

For the Degree of Doctor of Philosophy

Colorado State University

Fort Collins, Colorado

Spring 2024

Doctoral Committee:

Advisor: Jeff Hansen

Laurie Stargell
Tim Stasevich
Donald Mykles

ABSTRACT

REEXAMINING THE ROLE OF LINKER HISTONES BEYOND 30 NM FIBERS IN A COMPLEX CHROMATIN ENVIRONMENT

Eukaryotic cells store DNA in the cell nucleus in the form of chromatin. Chromatin is composed of nearly equal parts proteins and DNA. It is both highly compacted and organized into discrete domains within the nucleus. However, the manner in which chromatin is compacted, and domains are organized, remains elusive. The primary players in chromatin compaction are core histones, which bind DNA to form the nucleosome and the basis for 10 nm fibers. Linker histones also play an important role in chromatin compaction. Previous work showed that linker histones are important for the formation of 30 nm structures. 30 nm structures were long held to be folding intermediates for repressive chromatin domains. However, there is little evidence for these structures in most eukaryotic cell types. Instead, chromatin appears to be composed of an interdigitated 10 nm fibers in both repressive and accessible chromatin types. The role of linker histones in 10 nm fibers is not well characterized. Previous work showed that linker histones stabilized 30 nm structures, rendering them inaccessible to binding by additional proteins. In the following, we investigate the behavior of linker histones in an interdigitated 10 nm fiber environment. We use an *in vitro* model called “condensates” to mimic the formation of 200 nm chromatin domains. We find that linker histones stabilize these condensates by cross-linking chromatin fibers. Importantly, we show that the presence of linker histones does not preclude

binding by additional proteins. Linker histones readily bind condensates in ratios above an expected one linker histone per nucleosome. Additional binding by linker histones suggests that 10 nm fibers provide a complex environment in which linker histones dynamically interact with both nucleosomes and linker DNA.

ACKNOWLEDGEMENTS

There are many people I would like to acknowledge for their contributions to the completion of this work. First, I would like to thank my advisor, Jeff Hansen, and Student Advisory Committee members Laurie Stargell, Tim Stasevich, and Donald Mykles. Their contribution and support helped focus the direction of this greatly. I especially would like to acknowledge the contributions of our collaborator Curtis Alexander Davey. Curtis Davey provided us with all the linker histone variants that make up the crux of this study, without which this work would never have been completed. Additionally, I would like to thank Grant Schauer for providing us with polymerase ε to use in our assays. I also want to thank Ashley Oxford from the Schauer lab, who purified much of the polymerase ε we used.

I would like to thank several members of the Hansen lab for their individual guidance and contributions. Tommy Tolsma helped train me on the confocal microscope, and contributed fluorescence microscopy on the binding interaction between Pol ε and condensates. Kelly Britton and Walter Robles worked as excellent undergraduate researchers to support me in this work. Kelly Britton primarily worked on SirT6 binding assays, but also contributed to some of the BSA and salt dissociation assays. Walter Robles also worked on BSA assays with both Kelly and me.

Finally, I would like to thank Gabriel Galindo from the Stasevich lab. Gabriel wrote the python code that helped me quantify condensate sizes in bulk. Gabe also provided much appreciated company from time to time when I was working late at the microscope.

TABLE OF CONTENTS

Chapter 1

Introduction

A DNA molecule of the human genome, stretched from end to end is between 1 and 2 meters long. Compare this to the relative size of human cells, which varies from around 2 to 150 microns. We know that DNA must be highly compacted to fit into the nucleus of a human cell, and yet, it must also remain both organized, and accessible to the cell for transcription. On a large scale, for humans and the eukaryotic kingdom in general, genes are grouped into categories called chromosomes. Chromosomes were originally observed through simple light microscopy experiments, where DNA is easily stained, and can clearly be seen condensing into distinct structures during the process of cell division. However, during the rest of the interphase period, the nucleus appeared as a mostly dispersed and amorphous structure. So, how did the cell know how to organize its chromosomes? Light microscopy revealed that during interphase, structurally distinct “dark” and “light” regions could be observed, and these were dubbed “heterochromatin” and “euchromatin,” respectively (*4*). Likewise, euchromatin was deemed “active,” while heterochromatin, apparently much more dense in nature, deemed “inactive.” Later work using fluorescence in situ hybridization (FISH) microscopy showed that chromosomes remained as discrete entities within the nucleus, as apparent “territories” (*4*). Within mammalian chromosome territories, super-resolution microscopy also uncovered additional 200 nm globular structures called “domains” (*4*).

On the fundamental level, it was observed that a group of proteins called histones appeared highly involved in the folding and compaction of DNA. These histones bound each other and DNA to form nucleosomes, which appeared along an outstretched strand of DNA as “beads on a string” (*5*). *In vitro* studies showed that low levels of divalent cationic salts caused these arrays of nucleosomes to form cylindrical structures approximately 30 nm in size and so named the “30 nm fiber” (*6*). These 30 nm structures were hypothesized to be a folding intermediate necessary for the construction of condensed heterochromatin found in interphase chromosomes. Further, in addition to the core histones that make up the nucleosome, so-called “linker histones” were observed to bind and highly stabilize these 30 nm structures (*7*). Indeed, to this day, this model for chromatin folding and repression is found in modern introductory biochemistry and molecular biology textbooks (*8*). However, later work failed to find evidence for these structures *in vivo*. Instead, the interphase chromatin environment appeared to be composed of a much more complex network of fibers, even in heterochromatin, and not tightly wound into neat 30 nm fibers (*9*). Thus, the story of chromatin folding, and heterochromatin compaction, had to be reworked. Additionally, the supporting and repressive role of linker histones had to be reimagined. What is the real role they played in chromatin architecture, if not to stabilize repressive 30 nm fibers?

In Chapter 2, we will review the 30 nm folding paradigm and the evidence against it. We reexamine the role that linker histones, and the various variants, appear to play in chromatin construction and maintenance. We will also introduce an *in vitro* model for studying chromatin, called “condensates.” Condensates share many of the basic

characteristics observed with chromatin fibers *in vivo*, and more specifically chromatin domains. In Chapter 3, we will present the methods and materials used to carry out our investigation. In Chapter 4, we will present the results of our investigation of the role of linker histones using condensates as a model for chromatin. Here we find that linker histones appear highly involved in maintaining the structural stability of condensed chromatin. By acting as a type of “glue” between chromatin fibers, linker histones are implicated in the construction and maintenance of chromatin domains. Finally, in Chapter 5 we will review the findings of this study, and outline potential future directions.

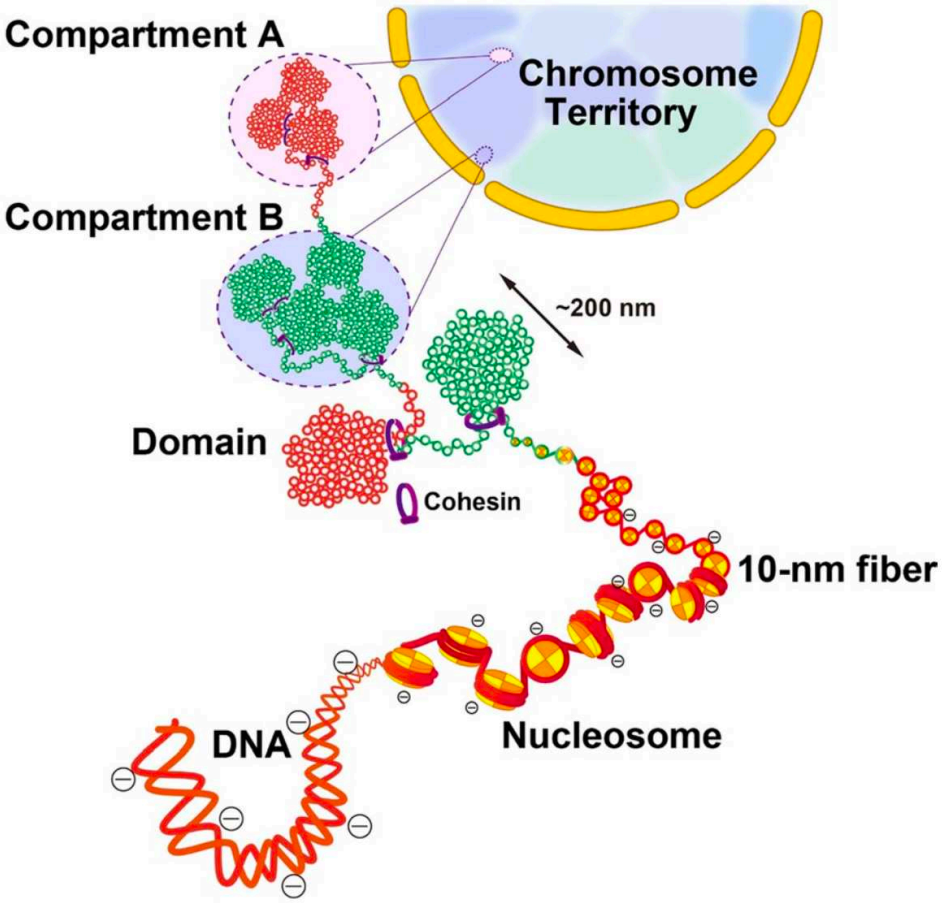

Figure 1.1: An Updated Simplified Model for DNA Organization into the Cell Nucleus. 10 nm fibers composed of nucleosomes compact into domains, which organize into transcriptionally active A and inactive B type compartments. This diagram was reproduced from Hansen et al. (*2*).

Chapter 2

Background on Chromatin, Linker Histones and Condensates

2.1 Introduction

The following chapter is broken into three main sections. In section *2.1* we review the basic structure of chromatin and chromatin domains and investigate how the 30 nm folding paradigm was both developed and overturned. In section 2.2, we review the structure and function of linker histones in chromatin, looking beyond the 30 nm fibers. Here we will focus on the role linker histones play in the maintenance of chromatin domains. Finally, in section 2.3 we present the condensate as an *in vitro* model for null chromatin and chromatin domains.

2.2 Overturning the 30 nm Fiber Folding Paradigm for Chromatin

The model for 30 nm fiber folding has become a widely accepted paradigm for how repressive chromatin fibers are condensed within the cell nucleus. However, researchers have not been able to confirm the existence of 30 nm fibers in both mitotic and heterochromatin across most eukaryotic cell types. In the following sections, we will introduce the basic make up of chromatin fibers, from core histones to the formation of 10 nm fibers and nucleosomes. We will review the 30 nm folding paradigm, as well as its flaws. Finally, we will introduce the current model for the 10 nm composition of chromatin fibers, in which includes both repressive heterochromatin and permissive euchromatin.

2.21 Core Histones and the Nucleosome

Chromatin is composed of equal proportions, by mass, of proteins, DNA, as well as some RNA (*10*). Histones are one of the most prevalent proteins that make up chromatin. Individually, histones are relatively small, only 11 to 21 kDa, and highly basic. Histones are rich in positively charged residues such as arginine and lysine, which constitute around 25% of their total amino acid composition (*8*). There are four "core" histones, including H2A, H2B, H3 and H4. H3 and H4 are strictly conserved across *Eukarya*, while histones H2A and H2B are much more variable across species (*8*).

H2A, H2B, H3 and H4 all contain a "histone-fold" domain (*11*). This domain is composed of three alpha helices and two loops; where loop 1 (L1) connects alpha helices 1 and 2 (α1 and α2), and loop 2 connects alpha helices 2 and 3 (α2 and α3)(*11*). The histone fold domain is integral to the formation of heterodimers between H2A and H2B, as well as H3 and H4 through the so-called "handshake motif" (*11*). The dimer interface found within the handshake motif is stabilized by hydrophobic interactions, hydrogen bonding and a number of electrostatic interactions (*11*). H2A-H2B and H3-H4 dimers further will form tetramers of $(H2A\text{-}H2B)_2$ and $(H3\text{-}H4)_2$, both of which further come together to make up the histone octamer which will define the very core of a nucleosome.

Nucleosomes are formed by the coiling of ~146 bp DNA around the octamer in an apparent superhelix (see Figure 2.1A) (*1*). The formation of the nucleosome is a stepwise process; first the $(H3\text{-}H4)_2$ tetramer binds DNA, which is followed by the association of dimers of H2A and H2B (*12*). Histone chaperones mediate and maintain

nucleosomes, including involvement in assembly and disassembly necessary for processes such as DNA repair and transcription (*8*).

An important feature of the nucleosome is formed by the interface of histones H2A and H2B to make up the “surface acidic patch” (*1*). This is characterized by a narrow groove where a cluster of eight negatively charged glutamic acid residues converge to form the so-called acidic patch (*13*). This negatively charged region is also flanked by a hydrophobic pocket, giving the acidic patch a distinct shape along with its electrostatic potential (*13*). Importantly, the acidic patch is able to accommodate a variety of binding motifs, and plays an important role in facilitating an interaction between adjacent nucleosomes by binding the tail domain of H4 (*13*).

Core histones contain N-terminal tail domains, which protrude from the nucleosome core into the surrounding solvent (*11*). These tail domains are flexible and unresolved in crystallographic depictions of the nucleosome (*1*). Core histone tail domains are enriched in positively charged lysine and arginine residues (*11*). Importantly, these domains are involved in interacting with adjacent nucleosomes via the acidic patch, linker DNA, and can also be modified by several post translational modifications (PTMs). PTMs can affect the characteristics of both their charge and shape (*11, 13*).

PTMs to the histones and their tails encapsulate what is known as the “histone code,” which likely regulates state of either transcriptionally active, or repressed, chromatin (*14*). The “histone code” is determined by the number, type of modification, as well as the particular residue to which they are attached (*14*). Possible PTMs include methylation, acetylation, phosphorylation, ubiquitination, etc. In addition to the four core

histones, there are also a number of additional histone variants that can replace H2A, H2B, H3 or H4. For example, variant H2A.Z is a variant involved in transcriptional regulation, while variant H2A.X is implicated in DNA damage and double-stranded break repairs (*11*).

2.22 The 10 nm Fiber

The association of DNA with histone octamers forms the 10 or 11 nm diameter structures that appear as “beads on a string” along a stretch of DNA. Each “bead” on these strings is a nucleosome, discussed in detail in the previous section. These 10 nm fibers make up the most fundamental structural component of a chromosome. Indeed, an interphase chromosome is essentially a single long 10 nm fiber (*4*). This coiling of DNA around the nucleosome contributes to > 6 fold compaction of the molecule, which unfortunately is still not enough to completely enfold the chromatin within a cell nucleus (*5*). Therefore, additional packaging into 30 nm fibers was proposed as a possible intermediate folding step in the formation of higher-order structures.

2.23 The Development of the 30 nm Folding Model

The first folding intermediate on the path from 10 nm fibers to higher order condensed chromosomes was long held to be 30 nm fibers. These fibers are composed of tightly wound helical structures around 30 nm in diameter, arranged with 1 linker histone per nucleosome (*7*). 30 nm fibers provide an additional 100 fold compaction of DNA on top of the nucleosome compaction (*15*). Why were these particular structures proposed as a folding intermediate? The answer has to do with the types of both *in vivo* and *in vitro* experiments that were run on chromatin from isolated nuclei. Early studies employed nuclease digestion followed by an elution in low salt conditions to obtain

hundreds of nucleosomes (*16*). Through electron microscopy (EM), researchers observed a salt-dependent folding of the isolated nucleosome arrays into fibers with an apparent 30 nm diameter structures (*16*). Transmission EM (TEM), atomic force microscopy and cryo-EM also showed that these 30 nm fibers were composed of irregularly arranged nucleosomes in a zig-zag orientation (*17*). The orientations observed also appeared dependent on the length of intervening linker DNA, even in the presence of divalent cations (*18*). Additionally, the formation of "stem" like motifs were observed through cryo-EM in the presence of linker histone, which promoted the juxtaposition of adjacent linker DNA and further compaction (*19*).

In addition to the isolated nucleosome arrays from nuclei, arrays were also constructed from recombinant histones and DNA using a controlled salt gradient through dialysis (*20*). Artificial construction of these arrays allowed for intentional and controlled nucleosome positioning, changes to core histone domains, elimination or addition of PTMs and linker histones (*20*). Sedimentation velocity experiments, along with EM experiments, then could be employed with great accuracy to determine the degree of compaction and folding under different experimental conditions. For example, nucleosome arrays composed of 12 repeats (12-mer) of nucleosomes along a DNA template are known to sediment around 29 to 30 S in low salt conditions (*21*). The 29 S sedimentation coefficient is matched to the apparent "beads on a string," or extended nucleosome array motif. With the addition of 1 mM $MgCl_2$ and linker histones, however, these arrays sediment around 60 S, and correspond to the tightly compacted 30 nm structures (*16*).

There were several proposed models for the exact orientation of nucleosomes and linker histones in these 30 nm fibers. The irregular folding model, pulling from observations from cryo-EM, suggested that nucleosomes orient themselves into zig-zags in 3D space, enfolding linker DNA into the interior of the fiber (*18, 19*). Additionally, from X-ray diffraction data, a solenoid model for nucleosome arrangement was put forth. The solenoid model suggested that each nucleosomes successively folded along linker DNA to form a helix, with about 6 nucleosomes per turn (*22*). There was also an interdigitated solenoid model proposed based on observations from EM on small chromatin fragments (*23, 24*). In this model, nucleosomes were said to interdigitate upon each helical turn of the solenoid, further stabilizing and compacting these structures.

Despite the *in vitro* observations, and multiple models for precise nucleosome arrangements, researchers struggled to find wide-spread examples of the 30 nm fibers *in vivo*. It was noted that these structures likely did not extend over the entire chromosome, but instead were associated with repressed or “closed” chromatin. On the other hand, “open” chromatin was believed to take on the 10 nm arrangement that intuitively appears more accessible and so, “active.” Therefore, transcriptionally “silent” chromatin, including heterochromatin, and metaphase chromatin, were by default assumed to fold into the intermediate 30 nm fibers, largely facilitated by the presence of linker histones.

2.24 Another Crack in the Model: Where are the 30 nm fibers?

Studies looking into 30 nm fibers hold more than a 30 year legacy in chromatin research. Although certain aspects of the model remained unrefined and even

controversial (*9*), the paradigm for 30 nm folding became well established in the much of the academic literature. It even became canonized in textbooks and introductory materials for high school and college students (*5, 8*). This began to change as more researchers questioned how relevant such structures must be if they are not widely observed in most eukaryotic cells.

In 2008 and 2010 Maeshima and Eltsov produced cryo-EM studies on human mitotic HeLa cells which showed that no evidence that 30 nm fibers were present (*25, 26*). In fact, as early as 1986, McDowall, Dubochet and colleagues published cryo-EM on metaphase Chinese hamster ovary (CHO) and HeLa cells which showed only 11 nm filaments, with no higher order superstructures observed (*27*). Both Maeshima et al., and McDowall et al., observed a largely homogenously grainy composition of chromatin fibers, where higher order structures were conspicuously absent (*25, 28*). Mcdowall et al. noted that nucleosomes appeared to be interacting together in a manner reminiscent of a liquid (*27*).

Further cryo-EM investigations revealed that heterochromatic regions looked much the same as mitotic chromosomes (*28, 29*). Similarly, cryo-EM on interphase eukaryotic nuclei also showed no signs of higher order structures beyond the 10 nm fibers (*9, 29, 30*). A combination of spectroscopic and tomography analysis on mouse interphase chromosomes produced a 3D representation encompassing both “open” and “closed” chromatin domains (*31*). Both domains showed no signs of 30 nm fibers, and appeared to be composed of 10 nm fibers only (*31*).

It has been reported that specific cell types, such as chicken erythrocytes and starfish spermatozoids do appear to contain 30 nm fibers (*25, 32*). This possibly suggests that

30 nm fibers may be important in terminal differentiation, or else exist only temporarily in highly localized areas (*4*).

2.25 A New Model: Chromatin Domains and the Interdigitated 10 nm fiber

In 2010, Maeshima and Eltsov suggest that instead of 30 nm fibers, compacted chromatin is likely composed of a network of irregularly folded nucleosome fibers, cross-linked by condensins (*25*). Further, they suggest that interphase nuclei are composed of numerous large “compact melt domains,” and “chromosome clumps” whose folding is driven by charge neutralization effects (*25*).

Work by Ou et. al. appears to validate many of the predictions Maeshima and Eltsov put forth. A technique called chromEM tomography (ChromEMT) uses fluorescent DNA binding dye Draq5, which has 14 binding sites per nucleosome, to increase the contrast of DNA (*33*). Ou et al. used chromEMT on mitotic and interphase chromosomes, and showed nucleosomes appeared to assemble into chains with diameters between 5 and 24 nm, in various conformations and arrangements (*33*). Ou et al. noted that areas of low densities of chromatin appeared as 10 nm fibers, with apparent “beads on a string” structures observed. On the other hand, the higher density regions of chromatin showed a much greater variety of conformations; including stacked nucleosomes, helical twists, and loops. Mitotic chromosomes showed that chains appeared compacted by a number of unstained scaffolding proteins (*33*).

Using a combination of super-resolution microscopy and computer simulations, Ricci et al. showed nucleosomes forming various “clutches,” or domains of different sizes, interspersed with nucleosome depleted regions (*34*). They found that pluripotent stem cells had fewer of the dense clutches. Additionally, the heterochromatin regions

were found to have linker histone H1 at elevated levels relative to smaller or nucleosome depleted clutches. Their observation suggests that areas of heterochromatin may be characterized by the formation of large dense clutches of nucleosomes, also containing a greater ratio of H1 than surrounding regions of euchromatin.

In a 2018 review, Hansen and Maeshima proposed several key predictions as to the organization of the interphase chromatin. First, they propose that the “default” conformation of chromatin, including condensed chromatin, appears to be composed of 10 nm fibers. These 10 nm fibers are likely in a variety of secondary conformations as an “interdigitated polymer melt” (*4*). Second, a nucleosome-nucleosome interaction forms the basis for this assembly; histone tails mediate the interactions between adjacent nucleosomes and linker DNA. This would make these structures particularly sensitive to histone tail modifications. Importantly, due to the weak interaction of H3 and H4 tails, this nucleosome-nucleosome association is likely dynamic, and fluid like. Third, these 10 nm fibers are further organized into chromatin domains which associate to form compartments, through extensive interactions and interdigitation. Heterochromatin rich regions would show evidence for more domain formation, as well as reduced dynamic or fluid like movement (*4*). Further, domains may be “molded” into functional compartments by the actions of linker histones, PTMs, histone variants, and additional chromosomal architectural proteins (*4*).

2.3 An Overview of Linker Histones and Their Role in Chromatin

Along with core histones, linker histones are one of the most common types of protein families found in eukaryotic chromatin. Linker histones interact extensively with

the nucleosome, and are believed to play an important role in chromatin architecture and in the compaction of heterochromatin (*35*). Linker histones may also play a role in epigenetic regulation, DNA stability and repair, as well as regulation of DNA replication (*36*). Linker histones likely have additional binding partners beyond the nucleosome, and are subject to regulation through a variety of post-translational modifications (PTMs), although all the players involved are not very well characterized (*36*). 11 linker histone variants have been found in both mice and humans. Seven of the variants are somatic and include H1.0, H1x, as well as H1.1 through H1.5. Variants H1.1 through H1.5 are also known as H1a through H1e respectively, however we will refer to their numerical nomenclature from here on (*37*). Additionally, there are three testes-specific variants, (H1t, H1t2, HILS1) and one oocyte specific (H1oo) (*36*).

2.31 Linker Histone Structure

Linker histones variants share a fairly conserved overall tripartite structure consisting of three domains (*36, 38*). Human somatic variants H1.1 through H1.5 share more than 66% amino acid sequence overlap, while H1x and H1.0 share between ~30% to ~40% sequence similarity overall with all other somatic variants (see table 2.1). The most highly conserved area among all the variants is the central globular domain, which forms a DNA binding winged helix consisting of about 75 amino acids (*39, 40*). The central globular domain is surrounded by two intrinsically disordered domains; the short N-terminal tail domain, and a longer (~100 amino acids), C-terminal tail domain (CTD) (*41*). While both N- and C- tail domains vary in length and sequence among variants, generally the N-terminal domain is shorter and more hydrophobically enriched than the CTD (*41*).The CTD generally displays highly basic characteristics, and is typically

composed of approximately 30% to 50% positively charged residues (*38*). Additionally, the CTDs appear rich in proline residues, potentially preventing further folding in solution (*38*). No structures of the CTD have been observed either through X-ray crystallography nor cryo-electron microscopy (cryo-EM) (*40*). However, trifluoroethanol has may induce the formation of an alpha helix structure in the CTD, as observed through circular dichroism (CD), infrared spectroscopy (IR), and NMR (*38*). Additionally, the interaction between the linker histone CTD and DNA in solution appears to induce the formation of secondary structures, including random coils (*38*).

2.32 Linker Histones and Chromatin

Linker histones are thought to regulate DNA accessibility by binding nucleosomes and altering chromatin structure (*7, 16, 42*). Much work had been done to show how linker histones stabilize the 30 nm fibers in solution (*4, 7, 16, 19, 42*). Previous work showed that linker histones bind nucleosomes at a 1:1 ratio H1/nucleosome at the entry and exit site of linker DNA or “on-dyad” (*36*). In addition to X-ray crystallography, Cryo-EM structures also showed H1 bound to the nucleosome on-dyad with its CTD electron density interacting with adjacent linker DNA (*43*). In 30 nm fibers, linker histones stabilize condensed stacks of nucleosomes into coils with the additional interaction through the CTD and the linker DNA (*19, 36*). In this model, accessibility to DNA binding sites only opens when linker histones are removed from chromatin, facilitating the unravelling of tightly wound 30 nm fibers (*36*). However, less is known how linker histones behave in the interdigitated 10-nm fiber environment.

Recent evidence suggests linker histones may indeed exhibit multiple distinct binding interactions with nucleosomes and linker DNA. In a 2014 cryo-EM study,

tetranucleosome arrays were shown in repeating tightly packed stacks of 30 nm fibers, where the linker histone was shown in a 1:1 ratio with nucleosomes and facilitating a left-handed twist (*44*). However, a 2020 crystallography study by Davey et al., two distinct binding modes for H1.0 were shown (*45*). The on-dyad mode that was seen in earlier studies was observed, as well as a more remote 'non-dyad' mode (*45*). In the non-dyad binding mode, the globular domain resides in a pocket of nucleosomes, interacting with nucleosome core DNA from three separate fibers— further solidifying the interdigitation of the nucleosome network (*45*).

The globular domain of the linker histone is highly conserved, suggesting a small difference in the number and residue type may be responsible for different binding modes. Other studies have shown that the variable and highly charged C-terminal domain of linker histones serves as a stabilizing factor for linker DNA, suggesting its variations may promote different higher-order structures (*46-48*). Furthermore, it may be that the folded higher-order structure of the nucleosome arrays effects linker DNA in such a way that the expected on-dyad binding mode can be disrupted (*36*). In fact, the highly disordered region of the linker histone CTD has been proposed to act as a "liquid-like glue" between chromatin fibers by cross-linking of different segments of linker DNA (*40*). Within the nucleus it is known the linker histones exhibit a great degree of mobility (*49*). This mobility may be driven by the non-specific binding interactions between linker histone CTDs and DNA, and moderate binding affinity between the globular domain and nucleosomes (*40*). The non-specific binding by the CTD may allow linker histones to slide around chromatin in a "liquid" like manner, from nucleosome to nucleosome (*40*).

Therefore, linker histones are not stabilizing chromatin by forming “fixed” inaccessible coiled structures, but instead through a more dynamic stabilization of adjacent fibers.

2.33 Linker Histones and Additional Protein-Protein Interactions

In addition to their interaction with nucleosomes, linker histones are likely involved in interactions with a complex number of histone chaperones, transcription factors, and downstream DNA damage repair factors (*50*). For example, H1-depleted mouse embryonic stem cells (mESCs) showed an increased sensitivity to DNA damage (*36*). Importantly, H1 is a known target of E2 ubiquitin-conjugating enzyme UBE2N, which works in the double-stranded breaks (DSBs) signaling pathway that recruits DNA repair factors (*36*). Affinity binding interactions using immobilized H1.0 and nucleolar extracts identified at least 175 different proteins bound (*50*). Interestingly, with the removal of the CTD of H1.0, 25% of these interactions were completely wiped out (*50*). This indicates that the CTD of H1 may play a role in modulating additional protein-protein interactions in chromatin. This is further highlighted by the numerous post-translational modifications (PTMs) H1 can undergo, many of which also occur on the CTD.

H1 may take on various PTMs, including phosphorylation, methylation, and acetylation (*36*). Notably, the level of H1 phosphorylation is regulated by the cell cycle; it displays low levels during G1 phase, higher levels during S and G2 phases, and reaches its maximum during metaphase (*36*). However, how phosphorylation effects H1 activity is complex, depending on which residue it occurs to. For example phosphorylated Ser172 on H1.2 and H1.5 localizes each to active DNA replication foci

and transcription sites to facilitate silencing, where phosphorylation of Thr146 of H1.2 causes its dissociation from p53 thus activating p53 genes (*36*).

Polycomb repressive complex 2 (PRC2) is a complex that aids in chromatin compaction through methylation of H3K27(*51*). Wilcockson et al. used reconstituted dinucleosomes to show that H1 strongly promotes PRC2 H3K27 methylation (*52*). Linker histones also have direct interactions with methyltransferases Suv39h1, Suv39h2, and SETDB1 (*53*). These methyltransferases are responsible for the H3 lysine 9 (H3K9) trimethylation of chromatin, which is a marker for transcriptionally silenced heterochromatin (*35*). Not only does H1 bind Suv39h1, Suv39h2, and SETDB1, but may further promote methyltransferase activity (*35*). *In vitro* studies using reconstituted dinucleosomes showed that H1 bound nucleosomes showed greater enzymatic activity than those without. This stimulation effect may be explained by the fact that H1 was shown bound to nucleosomes, while using its CTD to interact with either Suv39h1/2 as well as SETDB1 (*35*).

2.34 Linker Histones and TADs

Topologically associated domains (TADs) are continuous regions of chromatin that can range from 100 kb to 10 Mb of DNA. These are conserved regions identified through chromatin conformation capture (Hi-C) studies which show a greater degree of DNA-DNA interactions found within the domains than without (*36*). Domains have also been confirmed visually using super-resolution microscopy and appear to correspond with the same 200 nm domains observed previously through both light and electron microscopy (*54*). These domains are generally further organized into two distinct

compartments A and B, where A may represent transcriptionally active chromatin, and B transcriptionally repressed (*54*).

Triple knockout H1.2, H1.3 and H1.4 of mESCs showed TADs had increased frequency of inter-domain contacts, with little to no changes observed in either their size or location (*36*). Additionally, the nearly 50% decrease in linker histone levels changed the epigenetic landscape by altering levels of activating H3K4me1/3 at various loci and increasing DNA hypersensitivity sites (DHSs) suggestive of chromatin decompaction (*36*).

Further, a triple knockout-of H1.3, H1.4 and H1.5 on mESCs, showed that the H1 depletion led to increased B to A compartment shifting, characterized by increased DNA contacts between compartments (*52*). Willcockson et al. reports that the local density of H1 plays a critical role in the maintenance of discrete compartments; with H1 rich compacted compartments promoting the repressive H3K27 marks, while reducing more accessible H3K36 marks (*52*). Therefore, it seems H1 plays a critical role in constructing discrete chromatin domains through compaction, which may serve to further recruit additional heterochromatin associated proteins to assist in the silencing of specific regions of the genome.

2.4 Condensates as Models for Chromatin

We know that chromatin fibers are likely composed of an interdigitated network of 10 nm fibers, which may further become compacted into discrete domains. This network is very likely mediated by the interactions between adjacent nucleosomes through their tails and the surface acidic patch. We propose that chromatin domains are therefore

assembled in two basic ways: 1) through the self-interacting characteristics of the chromatin fiber itself, and 2) by chromosomal proteins that help mediate the self-interacting properties of the chromatin fiber through binding interactions and PTMs to form organized structures with specific functions. In the presence of divalent cations, nucleosome arrays will fold to form a structure referred to here as “condensates.” In the following, we present condensates as an *in vitro* model for chromatin domains.

2.41 Divalent Cations Facilitate Chromatin Condensation and Condensate Formation

Much work has been done to show that divalent cations are necessary to the process of chromatin condensation. High resolution X-ray crystallography studies show both mono- and divalent cations bound to the nucleosome core (*55, 56*). Additionally, significant changes to chromosome structure have been observed when there are changes to the concentration of cations. For example, heterochromatin only appears present in nuclei if the concentration of Mg^{2+} is greater than or equal to 2 mM, and lower salt causes chromatin to decondense (*57*). The greatest degree of compaction occurs in the presence of either Mg^{2+} or Ca^{2+}, and this process is reversible upon removal or addition of salts (*57*). In 2001, Strick et al. mapped the distribution of cations present in interphase and metaphase chromosomes (*58*). They found that Na^{+} and K^{+} do not appear to redistribute during the cell cycle, however, the concentration of Mg^{2+} and Ca^{2+} increases to about 12 to 22 mM and 20 to 30 mM respectively (*58*).

Schwarz and Hansen et al. found that nucleosome arrays equilibrate between folded, and unfolded states in conditions under 2 mM $MgCl_2$ (*6*). In 2016, Maeshima and Rogge et al. showed that titrating between 0.5 and 2 mM Mg^{2+} caused arrays to fold into

helical 30 nm fibers. Between 2 and 4 mM Mg^{2+} a greater degree of self-association was seen, with the formation of supramolecular “oligomers,” which are equivalent with what we are referring to as “condensates” (*59*).

Divalent cations appear to work with the tail domains from the core histones to facilitate this reversible self-association found in nucleosome arrays (*57*). The cations likely do this in part by helping to neutralize the charge of intervening linker DNA. In addition, the cation type also matters for facilitating these self-association properties. Monovalent salts such as Na^{+} were actually shown to reduce the degree of self-association, even in the presence of divalent cations such as Mg^{2+} (*57*). This suggests that there may be some competition between mono- and divalent salts in binding linker DNA.

2.42 Core Histone Tails Are Essential to Condensate Formation

Tail domains from the core histones are essential to the self-association of nucleosome arrays. Naked DNA does not show the same self-association properties under the same ionic conditions used for condensates(*4*). Similarly, the degree of octamer saturation on a DNA template is sensitive to the relative concentration of $MgCl_2$ introduced, requiring higher concentrations of Mg^{2+} for folding relative to fully saturated templates. The removal of the tails through trypsinization, even in the presence of $MgCl_2$, abolished all self-association folding effects (*57*). In 2005, Gordon et al. showed that all four core histone tail domains independently contribute to condensate assembly in an additive manner (*60*).

Additional work showed that the nucleosome to nucleosome association seen in condensates is sensitive to tail modifications. Mishra et. al. showed that even a change

to the tail domains on a single nucleosome within the middle of 25-mer nucleosome arrays can show changes to self-association (*61*). Mishra et al. used an acetylation mimic on the H4 tail domain, and its addition showed increased accessibility to the surrounding linker DNA. This effect was enhanced with the addition of H3 acetylation tail mimics; though the introduction of H3 mimics on their own appeared to have little effect (*61*).

2.43 Condensate Morphology and Packaging

Fluorescent microscopy and TEM reveal that condensates have a spherical or "globular" overall shape, with a distribution size ranging from ~100 to 1000 nm (*59*). The average density of DNA per condensate varied from 1Mb to 500Mb, from domain to chromosome size (*59*). Analytical ultracentrifugation showed these structures had sedimentation coefficients ranging from 10 to 100,000 S. These structures were only observed in concentrations of 4.5 and 10 mM $MgCl_2$, with none appearing in concentrations ranging from 0 to 1.5 mM $MgCl_2$. Further, TEM showed globular structures around 200 nm radii at both 4.5 and 10 mM $MgCl_2$. Importantly, the surface of the structure was not smooth; individual nucleosomes are visible in tightly packed 10 nm fibers (*59*). No 30 nm fibers or any other regular features are found in these structures. In addition to microscopy, small angle x-ray (SAX) analysis also showed the condensates were primarily composed of 10 nm fibers, and found no evidence for 30 nm structures, even when H1 was also present. 601x12 arrays with regular spacing and 5S sequences were both observed to form the globular structures, suggesting that their formation is not dependent on the spacing of the nucleosomes.

2.44 Liquid or Solid?

Debate remains whether chromatin exists in either a liquid or solid state, and if liquid-liquid phase separation (LIps) contributes to how higher order domains are regulated (*62, 63*). Under conditions with Mg Acetate cations and BSA, Gibson et al. showed that nucleosome arrays formed large ~1000 um condensates that displayed liquid like behavior (*63*). However, Strickfaden et al. looked at the physical state of condensed chromatin both *in vitro*, using reconstituted nucleosome arrays, and *in vivo* in live cells and found that chromatin behaved more like a solid (*62*). *In vitro,* chromatin condensates formed under a wide range of salt conditions were subjected to fluorescence recovery after photobleaching (FRAP) showed extremely slow, to no recovery, indicating a lack of mixing between bleached and unbeached chromatin (*62*). These condensates did not show any signs of fusing to form larger spherical condensates or droplets on contact as Gibson et al. had showed, but instead a more complex network of 3D structures, suggesting solid-like behavior (*62, 63*).

Likewise, *in vivo,* mobility tracking of fluorescently labeled nucleotides in genomic DNA showed that both in hetero- and euchromatin domains, the DNA appeared confined (*62*). Importantly, these domains did not show mixing with chromatin in the environment, even under hyperacetylated and decondensed conditions (*62*). Interestingly, the solid-like behavior of chromatin appeared to induce the formation of liquid protein condensates for a select number of heterochromatin proteins (*62*).

A study by Nozaki et al. suggests that chromatin displays “viscoelastic properties,” or that the physical properties observed are dependent on time and size scales used in its measurement (*54*). Indeed, Nozaki et al. found that on a local scale,

(nm/seconds) nucleosomes appear to dynamically fluctuate within domains in a liquid-like manner (*54*). However, at more global, or chromosome levels (um/minutes) the chromatin behaves more like a stable solid, also confirming the earlier work by Strickfaden whose study was conducted at the um and minute scale (*54*). The ability of chromatin to take on both liquid and solid-like properties on different scales may be a contributing factor to how it can be organized within the cell nucleus.

2.45 Condensates and Chromatin Domains

Hi-C studies have identified TADs as conserved higher-order chromatin structures characterized by increased the frequency of DNA-DNA contacts (*36*). In addition, ~200 nm globular domains have been observed using a variety of microscopy techniques (*64*). Chromatin within domains is made up of 10 nm fibers in an interdigitated network of nucleosomes. This nucleosome-nucleosome interaction forms the very basis for how higher order chromatin domains are formed. Nucleosome-nucleosome interactions are mediated in part by the histone tails, facilitated by the presence of divalent cation salts. Live cell super-resolution imaging showed that histone tail acetylation leads to decondensed chromatin domains (*64*). The individual contributions of the tails to adjacent nucleosomes are likely weak, transient, and fluctuating, implying they form a liquid-like packaging in chromatin (*65*). This fluctuating, liquid like movement of nucleosomes has been verified by Nozaki et al. through single nucleosome tracking in nm regions over seconds. On the other hand, the same study showed that FRAP analysis on similar chromatin in micrometer regions over minutes showed no recovery, indicating that at this scale chromatin behaves like a solid. In

addition heterochromatin rich regions showed the formation of more domains and showed fewer dynamic movements (*64*).

Condensates share nearly all the intrinsic properties of chromatin domains. They are condensed through a combination of divalent cation salts and histone tail interactions between nucleosomes. They show interdigitated 10 nm packaging widely found in *in vivo* microscopic analysis. Therefore, we propose that condensates serve as *in vitro* models for chromatin domains.

Condensates serve as highly valuable model systems for the behavior of chromatin domains as nearly every aspect of their formation is under a researcher's control. They can be used to investigate the various effects of histone modifications, histone variant substitutions, changes to the length of linker DNA, as well as the individual effects of additional chromosomal proteins on chromatin architecture.

Table 2.1: Clustal Omega Protein Sequence Alignment and % Sequence Overlap of Human Somatic Linker Histone Isoforms.

	H1x	H1.0	H1.1	H1.2	H1.3	H1.4	H1.5
H1x	100.00%	31.10%	33.51%	31.22%	31.05%	32.45%	31.58%
H1.0	31.10%	100.00%	42.77%	39.53%	39.66%	42.37%	36.87%
H1.1	33.51%	42.77%	100.00%	67.80%	67.61%	71.09%	66.98%
H1.2	31.22%	39.53%	67.80%	100.00%	81.69%	87.26%	80.00%
H1.3	31.05%	39.66%	66.98%	81.69%	100.00%	86.30%	77.06%
H1.4	32.45%	42.37%	67.80%	87.26%	86.30%	100.00%	86.11%
H1.5	31.58%	36.87%	71.09%	80.00%	77.06%	86.11%	100.00%

A

B

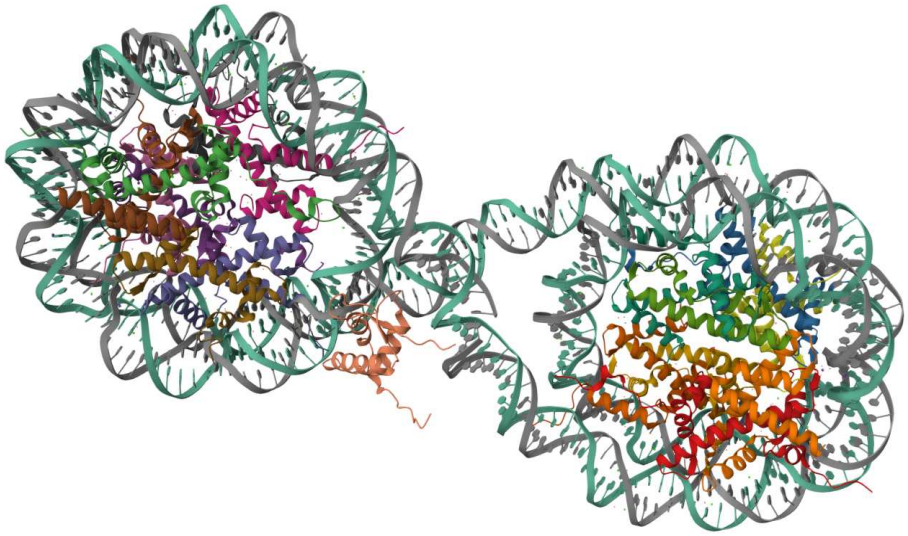

Figure 2.1: Structure of the Nucleosome Core Particle and Di-nucleosomes in complex with H1x.
A: 2.8 A X-ray crystallographic structure of the nucleosome core particle by Luger et al. (*1*) Nucleosome core assembled of 146 bp DNA wrapped around H2A (grey, gold), H2B (red, blue), H3 (pink, lavender), H4 (green, yellow). PDB id:1AO1.
B: 2.5 A X-ray crystallographic structure of di-nucleosome shown with H1x by Adhireksan et al.(*3*) H1.x is shown in orange at the interface (on-dyad) between adjacent nucleosomes. PDB id: 6L9Z

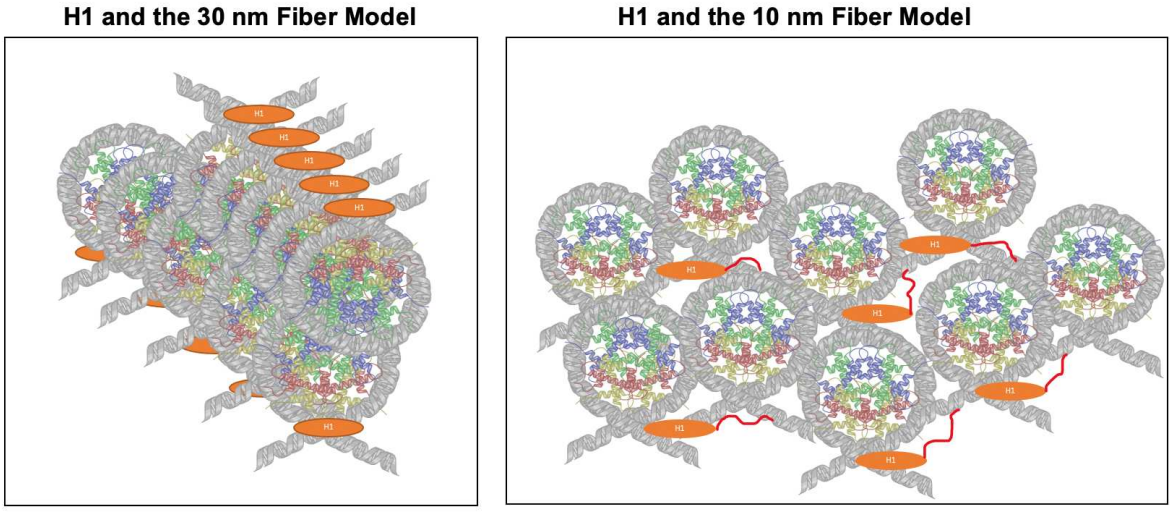

Figure 2.2: A comparison of H1 binding modes in a 30 nm fiber environment vs. 10 nm fibers. In the 30 nm fiber, linker histones facilitate the tight packing of nucleosomes into an inaccessible structure. In 10 nm fibers, linker histone binding is likely more fluid and dynamically driven by C-terminal tails (shown in red).

Chapter 3

Materials & Methods

3.1 Introduction

Condensates are formed from the divalent cation induced self-association of nucleosomes in nucleosome arrays. Widom et al. found that histone octamers have preferential affinity for certain sequences (*66*). This was done by combining affinity binding experiments over an extensive library of synthetic DNA sequences, in a series known as SELEX experiments (*66*). The “601” sequence developed by Widom et al. allows for accurate positioning of nucleosomes along a DNA template. Our condensates are formed from 12 “12-mer” nucleosome arrays, composed of 12 nucleosome repeats. These arrays are generated from a combination of reconstituted histone octamers, and a DNA template containing the 601 high affinity nucleosome positioning sequence discovered by Widom et. al. (*66*) . Once arrays are generated, they can be used to form condensates with the addition of divalent cation salts. The condensates themselves then can be used in subsequent experiments involving additional proteins such as linker histones.

3.11 Purification of 601x 12 Template Nucleosome Positioning DNA

DNA plasmids pUC19, containing 12 207 bp tandem repeats containing the 601 Widom nucleosome binding sequence (*66*) and ~63 bp linker DNA (see Appendix Figure 8) were initially transformed into dh5α cells. The 601x12 insert is located between the HindIII at position 2923 bp and XbaI at position 423 bp cut sites. Plasmid DNA was isolated using New England Biolab Monarch Plasmid Miniprep kit, typically

resulting in 40-90 ng purified plasmid. To verify the presence of the desired insert, restriction enzyme digest using a combination of Xba1, HindIII, HaeII and Dra1 (New England Bio labs), was used on purified plasmids. The presence of a ~2500 bp band is indicative of the presence of the 601x12 insert found between XbaI and HindIII cut sites, along with 4 additional bands representing the remaining digested plasmid from additional restriction enzyme cut sites (see figure 3.1A). Newly transformed plasmid was inoculated into 20 mL TB and 100 ug/mL Ampicillin and used for glycerol stocks, followed by a large-scale inoculation into 6 liters Ampicillin+ TB. Subsequent plasmid was purified from *E.coli* through an alkaline lysis procedure. Plasmid containing a 2467 bp insert digested using Xba1 and HindIII to cut out the template, and HaeII and Dra1 further digested the remaining plasmid fragments. Digested plasmid fragments were separated through size exclusion chromatography on a Sephacryl S-1000 column (see figure 3.1B). Fractions containing the 601x12 2500 bp fragment were combined, and alcohol precipitated (see figure 1C). The template DNA was then resuspended in 10 mM Tris pH 7.8 and .1 mM EDTA buffer to 1 mg/mL.

3.12 Assembly and Purification of Histone Octamers

Recombinant *Xenopus* core histones H2A, H2B, H3 and H4 were purchased through the PEP facility at CSU. Octamer reconstitution was done according to the protocol originally described by Luger et al. in 1999 (*67*),with modifications according to Rogge et. al. (*68*). The lyophilized histones were resuspended in 6M guanidinium HCl, 20 mM Tris pH 7.5, and 5 mM DTT for 2 hours at 25°C. Next, histones were subsequently mixed at equimolar ratios at a final concentration of 1 mg/mL. The mixture was dialyzed against 2M NaCl, Tris pH 7.5, 1 mM EDTA, and 5 mM B-mercaptoethanol,

with fresh buffer being changed three times every 4 hours as described previously (*67*) . Folded octamers were concentrated using Amicon Ultra-15 centrifugal filters, and purified using size exclusion chromatography with a HiLoad 16/6- Superdex 200 column on the AKTA start liquid chromatography system with Unicorn software (see figure 3.1D). The molecular weights of *Xenopus* H2A and H2B only differ by 200 Da and so typically appear as a single band on SDS PAGE (*68*). H2A has a molecular weight of 13.96 kDa, H2B is 13.77 kDa, H3 is 15.27 kDa, and H4 is 11.24 kDa (*68*) Fractions collected from the peak were checked using SDS-PAGE (see figure 3.1E), then combined and concentrated using an Amicon Ultra 15 centrifuge filter to 5 mg/mL.

3.33 Alexa 488 and Alexa 647 H4E63C Labeling and Labeled Histone Octamer Assembly

Recombinant H4E63C was purchased from the PEP facility at CSU. The addition of the Alexa 488 or Alexa 647 fluorophore was done by adding equimolar concentration Alexa 488/647 C5 maleimide to histone H4E63C in 6M guanidinium HCl, 20 mM Tris pH 7.5, and 0.7 mM TCEP. The fluorophore and histone solution was covered and placed at 4° C overnight in a rotator. Fluorescently labeled H4 was then mixed with H2A, H2B, and H3C110A (to prevent additional fluorophore labeling) in equimolar ratios, and subjected to the same dialysis and size exclusion chromatography purification protocol described previously for unlabeled octamer assembly with the exception that the solution was kept in the dark at all times.

3.34 Alexa 488 H1.0V87C Labeling

H1.0V87C was generously provided by our collaborator Curtis Alexander Davey. H1.0V87C was suspended 10 mM Tris pH 7.5, 1 mM EDTA buffer and 10 mM TCEP

and mixed for 1 hour at 25°C. An equimolar ratio of Alexa 488 C5 maleimide was mixed with H1.0v87C, covered from light, and rotated at 4°C overnight. The resulting labeled H1.0V87C was then purified over a gravity controlled Sephadex G-25 HiTrap Desalting column. Fractions were analyzed using SDS-PAGE and fluorescent fractions containing H1.0V87C were combined. Pooled H1.0v87C was further concentrated to 2 mg/mL using Amicon-Ultra centrifugal filers.

3.35 Assembly of Unlabeled Nucleosome Arrays and Alexa 488 and Alexa 647 Labeled Nucleosome Arrays

Nuclesome arrays were prepared according to the protocol described by Rogge et al. in 2013 (*68*). Equimolar combinations of the purified 601x12 DNA template with reconstituted histone octamer to a final concentration of .3 mg/mL. Nucleosome positioning was controlled over a decreasing salt dialysis protocol at 4°C starting at 2M NaCl, 1M NaCl, .75 M NaCl and ending at 2.5 mM NaCl in 10 mM Tris pH 7.8, .25 mM EDTA, as described previously (*68*). Resulting arrays were sedimented using a Beckman XL-I analytical ultracentrifuge, and analyzed using UltraScanIII (see Figure 3.2C). Arrays that sediment between 27 and 30 S, which contain between 11 and 12 octamer/template (*69*) were subsequently used for experiments and as standards for mono-nucleosome digest.

3.36 Assembly of Alexa 488 Labeled H1.0V87C Bound Arrays

Alexa 488 labeled H1.0V87C was mixed with unlabeled nucleosome arrays at a 1:1 ratio of H1/N at 4°C for 3 hours. The resulting mixture was dialyzed against 25 mM

NaCl, 10 mM Tris pH 7.8 and 1 mM EDTA in the dark overnight to a final concentration of .3 mg/mL.

3.37 Chromatin Condensate Formation

Condensates were formed by adding arrays to a final concentration of 10 nM to a 10 mM Tris pH 7.8, 1 mM EDTA solution containing >4mM $MgCl_2$, incubated for 20 minutes at 25°C.

3.38 Mono-Nucleosome Digest and Gel Shift Binding Assay

To test the saturation nucleosomes on nucleosome arrays, as well as determine subsequent nucleosome binding by linker histones a mono-nucleosome digest was performed (see figure 3.2A and 3.2B) (*69*). First, condensates were formed as described above. Linker histone was added in increments of 10 ng up to 100 ng to 600 ng condensates and incubated for 15 to 20 minutes at 25°C. Eco-RI (New England Biolabs), at 12 U enzyme per 0.6 ug 601x12 DNA, was added to each sample at digested at 37°C for 75 minutes. Digestion was quenched using 35 mM EDTA and by placing samples on ice. Samples were electrophorized on 1% Agarose, and stained using ethidium bromide.

3.39 Micrococcal Nuclease Digest

3 ug 601x12 DNA was incubated in 4 mM $MgCl_2$, 0.1 mM $CaCl_2$, 2.5 mM NaCl, 10 mM Tris, pH 7.8 for 10-15 minutes at 4°C to fully self-associate. After self-association, linker histone H1.0 was added to the mixture at ratios of 1:1 and 2:1 H1/N. 12.5 U enzyme (~2.5 U enzyme per reaction time point) of Microcrococal Nuclease (Worthington Biochemical Corporation) was added and condensates digested at 37°C

for 0, 5, 10, 15, 20 and 30 minutes. Reactions were quenched using 10 mM EGTA and 35 mM EDTA and placed at 4°C. Digestion was verified using electrophoresis on 1% Agarose gel and visualized using ethidium bromide.

3.310 Differential Centrifugation Pelleting Assay

Following condensate formation, arrays were incubated with additional proteins, H1.0, H1.1, H1.3, H1.4, H1.5, Pol ε and SirT6 for up to 30 minutes at 25°C. Linker histone variants and SirT6 were generously provided by Curtis Alexander Davey, and Pol ε from Grant Schauer at Colorado State University. Pol ε was mixed at a ratios of .16, 0.75 and 1:1 pol ε/N. SirT6 was mixed with condensates at ratios of 0.5, 0.75, 1, 1.5, 2, 2.5, and 3 SirT6/N. Linker histones were mixed with condensates at input ratios (r^{H1}) H1: nucleosome of 0.25, 0.5, 0.7, 1, 1.5, 2, 2.5, 3, 3.5, 4, 4.5, 5, 5.5 and 6 to investigate different binding modes. After given binding time, condensate and protein mixtures were centrifuged at 20k rpm for 5 minutes. A sample of supernatant was removed and the pellet was subsequently washed with a 5mM $MgCl_2$ solution twice before pellet and supernatant were analyzed through SDS-PAGE.

3.311 Quantitation of Mole Ratios of Linker Histones and Nucleosomes

To analyze the amount of H1 bound to condensates, standards of known H1 (µg) along with the condensate pellets of various stoichiometries were run on SDS-PAGE, (Invitrogen Novex Wedgewell 4-20% Tris-Glycine Gels), and stained with Coomassie. Gel images were captured using ImageQuant LAS 500 (GE Healthcare, Chicago, IL, USA). Images were analyzed using the NIH public domain Java program ImageJ, utilizing the rolling ball background subtraction. Uncalibrated optical densities

(OD) were used to correlate protein loaded to peak areas using the equation described by Villela et al: P =C*V*1/2, where P is protein load in ng, C is concentration in mg/mL, and V is sample volume loaded in mL (*70*). Standard curves from the in-gel standards were generated for each gel using linear regression (Y=Uncal OD vs. X=protein load in ug) with $R^2 > 0.95$. and subsequent slopes were used to determine the amount of protein in µg. Protein amounts in µg were converted to moles using MW (g/mol) and mole ratios expressed as moles H1/ moles nucleosome.

3.312 Fluorescence Microscopy

Condensate samples were incubated with additional proteins (linker histones, SirT6 or Pol ε) and covered. Condensate samples were then placed on a MatTek glass bottom 35 mm petri dish with a 14 mm microwell 1.5 cover glass (MatTek, Ashland, MA, USA), and given an additional 20 minutes incubation and settling time. Condensates were imaged using Olympus IX81 spinning disk confocal microscope with photometrics Cascade II and a 100x/1.40 numerical aperture objective and Zeiss LSM 900 Confocal Microscope with Airyscan 2, with a 63x/1.40 objective/numerical aperture (Zeiss, White Plains, NY, USA). Slidebook 6 and Zen 3.1 software was used for both capture and image analysis. Quantitation of condensate size was done using matplotlib.pyplot, and python code developed by Gabriel Galindo at Colorado State University. Linked and connected condensates were meaured as one continuous condensate using thresholding and a rectanglar map drawn around “segmented coins.”

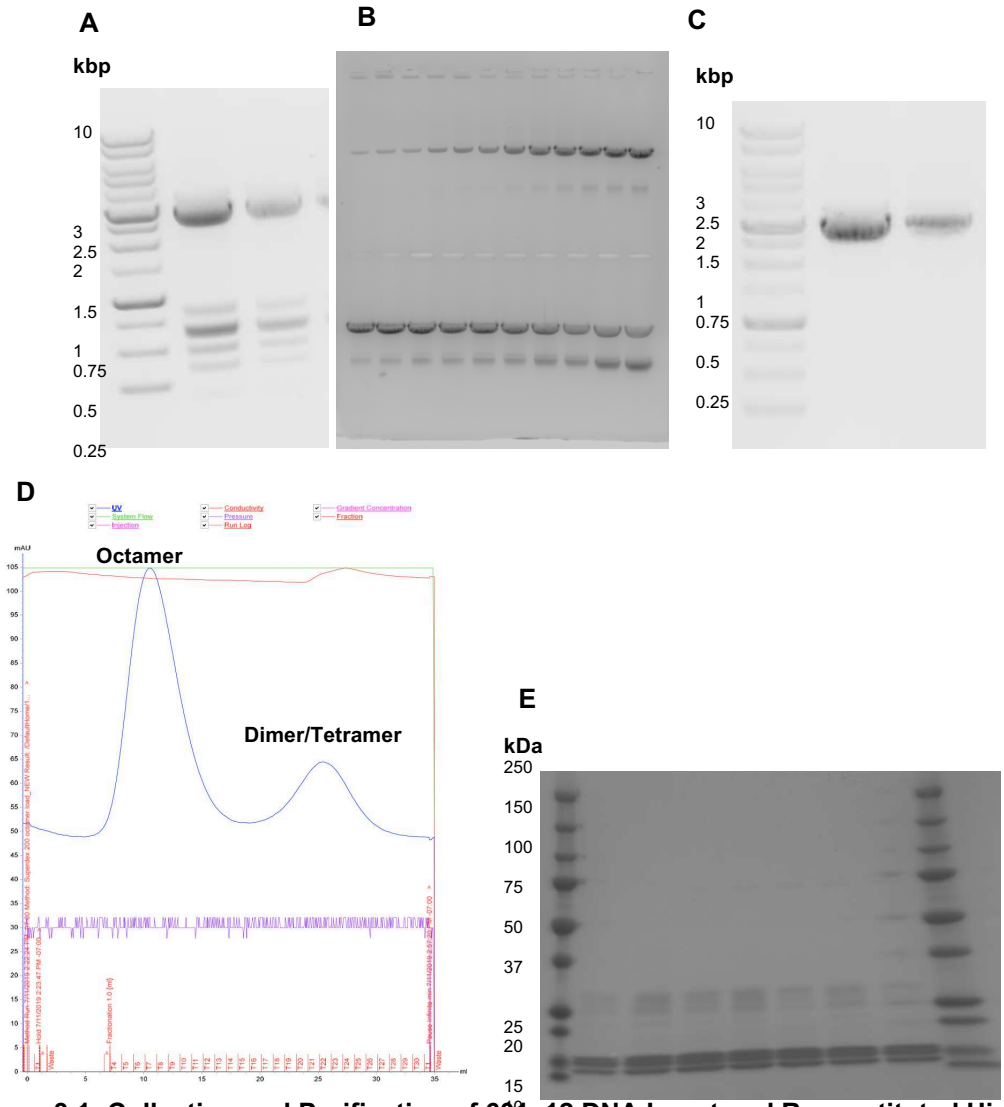

Figure 3.1: Collection and Purification of 601x12 DNA Insert and Reconstituted Histone Octamers Using Size Exclusion Column Fractionation. A: 1% Agarose gel, stained with ethidium bromide, shows the digestion of pUC19 plasmid containing 2467 bp 601x12 insert using restriction enzymes HindIII, XbaI, DraI and HaeII. The insert band appears around 2500 bp mark, while remaining plasmid fragments appear as smaller bands below (Goldbio 1 kb ladder shown for reference) **B:** Fractions obtained through gravity separation using Sephacryl-1000 size exclusion column. The ~ 2500 bp insert appears first, followed by additional plasmid fragments in later fractions. **C:** Purified 601x12 DNA insert shown following alcohol precipitation on 1% Agarose, stained using ethidium bromide.1 kb Goldbio DNA ladder is shown for reference. **D:** Chromatogram showing absorbance for fractions from reconstituted histone octamers. Fractions 5 through 11 show a peak representing the histone octamer, followed by a smaller peak including smaller tetramers and dimers. **E:** SDS PAGE showing collected fractions (5 through 11 shown in D). The core histones representing the octamer appear as 3 bands from 10 to 15 kD. Biorad Precision Plus All Blue Standards protein ladder shown for reference.

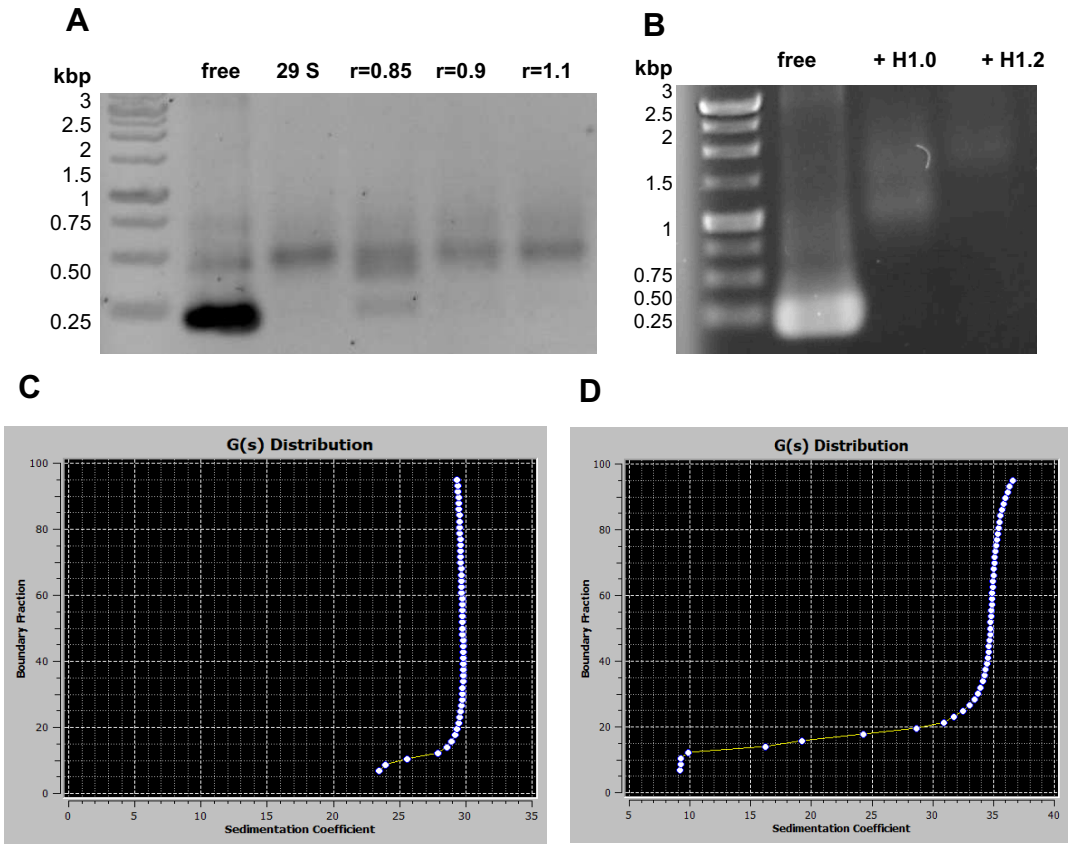

Figure 3.2: Assessing the Saturation of 601x12 Arrays and Binding of H1 to Arrays.
The saturation of the 601x12 DNA template with nucleosomes and linker histones can be tested using a mono-nucleosome digest along with analytical ultracentrifugation. **A:** Mono-nucleosome digest on fully saturated and under-saturated 12-mer nucleosome arrays. Lanes 1: GoldBio 1 kb DNA ladder, 2: Free shows 601x12 DNA digested in the absence of core histones, 3: 29 S represents nucleosome arrays analyzed previously by analytical ultracentrifugation and found to be 29 S (A1C) and, 4-6: Arrays with increasing ratios of core histones per Widom nucleosome positioning sequence shown as "r" from 0.85, 0.9, and 1.1. **B:** Mono-nucleosome digest on H1.0 and H1.2 bound arrays. Lanes 1: Goldbio 1kb DNA ladder, 2: Free 601x12 digested DNA, 3: H1.0 bound arrays, r^{H1}*=1.0* 4: H1.2 bound arrays r^{H1}*=1.2*. **C:** Distribution plot calculated following analytical ultracentrifugation showing fully saturated arrays sediment between 29-30S. **D:** Distribution plot following analytical ultracentrifugation of show H1.2 bound arrays of r^{H1}=1.2 sediment around 35 S.

Chapter 4

The Biochemical Basis for Compartment Formation

4.1 Introduction

Genomic DNA in Eukarya is highly compacted and organized by a number of proteins within the nucleus, forming chromatin (*4*). Nucleosomes make up the basic repeating structure of chromatin, and are composed of 147 bp of DNA wrapped around core histone octamer (*59*). Each histone octamer contains two copies of histones H2A, H2B, H3, and H4 (*59*). Nucleosome arrays are made up of nucleosomes repetitively spaced along the DNA (*59*). These arrays make up the 10-nm chromatin fiber (*4*). An interphase chromosome is composed of a single, long, highly organized 10-nm fiber (*4*). The mechanistic details into how the 10-nm fiber is both assembled and organized into an interphase chromosome is an active area of investigation. The aspects of chromatin packaging within an interphase chromosome may fundamentally illuminate how eukaryotic genomes are both organized and accessed, potentially furthering our understanding into gene expression (*4*).

Traditional models presented DNA packaging within the nucleus as helical, repetitive 30-nm fibers (*4, 32*). In low-divalent salt conditions, these 30-nm structures are well documented (*4, 32*). This model has been upended more recently, as cell nuclei do not appear to contain the 30-nm packaging in interphase chromatin. O'Shea and colleagues were able to visualize the 3D architecture of chromatin in situ using ChromEMT (*33*). They showed that interphase chromatin fibers appear as disordered 5 to 24 nm granular chains capable of a diversity of densities and structures (*33*). These

structures are likely dependent on a variety of factors, including variations in DNA sequence, DNA linker length, protein interactions, histone variants, and post translational modifications (*33*). Other studies using in situ, imaging, and small-angle x-ray scattering have suggested that the common repeating unit within chromatin adheres to 10-nm rather than 30-nm packaging (*59*). Nevertheless, the 30-nm packaging may be biologically relevant under certain conditions, such as terminal differentiation or transitional repressive structures (*32*).

Reconstituted chromatin structures known as “condensates” self-assemble into globular structures between 50-1000 nm in size in the presence of >2 mM $MgCl_2$ (*59*). The addition of Mg^{2+} ions to the arrays facilitates, along with the core histone tail domains, nucleosome-nucleosome interactions (*38*). In the presence of physiological range of Mg2+ (>2 mM Mg2+), these arrays self-associate to form larger chromatin structures called condensates. These structures appear to have nucleosome arrays packaged as interdigitated 10-nm fibers, and lack the canonical 30-nm packaging (*59*). Importantly, the formation of these condensates is reversible upon removal of the Mg^{2+} salt (*7, 59*).

There has been debate about whether chromatin is packaged in a liquid or solid state, and the role of liquid-liquid phase separation in domain formation (*62, 63*). Gibson et al. showed that nucleosome arrays formed large ~1000 um condensates that displayed liquid like behavior with the addition of Mg Acetate cations and BSA (*63*). However, Strickfaden et al. used FRAP on 601x12 condensates in 5 mM Mg^{2+} along with live cells and found that chromatin had slow recovery times, more indicative of solid-like behavior (*62*). Additionally, these condensates did not show any signs of

fusing to form larger spherical condensates or droplets on contact as Gibson et al. showed, but instead a more complex network of 3D structures, suggesting solid-like behavior (*62, 63*). A study in 2023 by Nozaki et al. suggests that chromatin is "viscoelastic" in nature, and displays both solid-like and liquid-like properties depending on the measurement scale used. Locally, Nozaki et al. showed that nucleosomes are highly dynamic within domains and behave much like a liquid (*54*). However, "globally," or at chromosome domain levels (um/minutes), the chromatin appeared to behave much more like a solid. The findings by Nozaki et al. also confirm the earlier work by Strickfaden, as the scale employed by both Strickfaden and Gibson were "global," using um and over the course of minutes (*54, 62, 63*).

The 601x12 chromatin condensates serve as an *in vitro* model, as they share many of the packaging and physical properties observed for *in vivo* chromatin. These condensates are therefore ideal for teasing out the most basic molecular and mechanistic properties of chromatin fiber structure and assembly. It is therefore possible to investigate intrinsic properties of chromatin using these condensates as a model. This can be done by adjusting parameters such as histone tail modifications and changing DNA linker length, as well as introducing extrinsic influencers, such as linker histones and other chromatin binding proteins and macromolecules.

Linker histone H1 is one of the most ubiquitous chromatin-associated proteins found among higher eukaryotes. Studies using X-ray crystallography show linker histones bind nucleosomes at the entry and exit site of linker DNA, or on the "dyad" axis of the nucleosome (*71*). Linker histones then affect chromatin fiber structure by apparently stabilizing locally folded secondary structures, as well as mediating the self-

association of these fibers by interacting with adjacent linker DNA (*41*). H1 bound arrays are typically associated with transcriptionally repressed chromatin fibers, and with the addition of different chromatin-associated proteins, may form different types of specific functional chromosomal domains (*7*).

Historically, the linker histones have been shown to induce and stabilize the formation of 30 nm fibers *in vitro,* though these fibers tend to show up only as short fragments interspersed with varying fiber sizes (*7, 36*). In interphase cells at 20 nm resolution, nucleosomes were observed to form discrete groups of varying densities called “clutches,” where increased linker histone presence were found in addition to other heterochromatin markers (*36*). Linker histone distribution has also been shown to be irregular within chromatin, where they tend to be depleted in promoter regions of actively transcribed genes with active histone marks (*36*). It has long been understood that linker histones likely alter chromatin architecture, thereby inhibiting access to DNA. This action includes preventing access to DNA binding proteins, and possibly preventing the processive action of DNA-tracking enzymes such as RNA and DNA polymerases and chromatin remodelers (*36*). Although H1 is generally assumed to be inhibitory by inducing 3D folding into higher order structures, such structures have also been shown to increase activity of a subset of nuclear enzymes such as PRC2, suggesting even these higher order structures are accessible to certain macromolecules (*36*).

In the following, we investigate the binding activity of linker histones to *in vitro* condensates using a combination of a gel shift assay, a biochemical pelleting assay, nuclease digestion, as well as fluorescence microscopy. We find that linker histones

readily bind nucleosomes in both linearized arrays and fully self-associated condensates. Additionally, when bound, linker histones appear to stabilize condensate structure via marked resistance to MNase digestion, as well as promoting self-association under both “liquid” and “solid” promoting conditions for condensates. Further, the presence of bound linker histones within condensates does not preclude the binding of additional chromosomal proteins. We show that linker histones can bind condensates above the traditional 1:1 H1 per nucleosome stoichiometry, with evidence for variant specific differences. This binding beyond the nucleosome also appears to mediate a condensate-to-condensate interaction. The density of linker histones found in chromatin may serve as an important factor in enhancing cross-linking and self-interaction properties found within chromatin compartments.

4.2 Results

4.21 Linker Histones Bind Nucleosomes in Linear Arrays and Condensates

To determine if linker histones can find and bind target nucleosomes within condensates, a mono-nucleosome digest was performed on both linearized arrays as well as fully associated arrays, or condensates. In the mono-nucleosome digest, any DNA that is unbound and accessible will be degraded by the addition of excess endonuclease EcoRI. Fully digested 601x12 nucleosome arrays will then appear as a band in an agarose gel around 500 bp, representing the bound nucleosome. The binding of linker histones to nucleosomes can also be detected by an apparent band shift under the same conditions. The high degree of charge present on the additional linker histone will cause the DNA band to present at a much higher length of DNA than without it present. In this way we can assess the degree of binding of additional linker

histones to arrays in linearized conditions, 0 mM Mg2+, as well as fully self-associated arrays, condensates, under conditions of 4 mM Mg2+ or higher. Here, we show that histone variants H1.0 and H1.5 bind nucleosomes in both condensates and linear arrays using the mono-nucleosome digest (figure 4.1A)**.** The addition of linker histones H1.0 and H1.5 was done in stepwise increments from 0 to 100 ng to a fixed amount of 601x12 arrays, incubated in either 0 or 5 mM Mg^{2+} prior to the introduction of linker histone. In figure 4.1A, H1.0 and H1.5 both show apparent binding at both 0 (linearized arrays) and 5 mM Mg^{2+} (condensates) above 50 ng H1. Indeed, H1.5 shows little difference in the degree of binding under both conditions. At 10 and 20 ng, H1.5 shows slightly more bound than at 5 mM Mg^{2+}, by 30 ng this difference is eliminated. On the other hand, H1.0 shows slightly less efficient binding under 0 mM Mg^{2+} than at 5 mM Mg^{2+} at lower levels of H1.0. However, under both conditions with H1.0, there are similar levels of binding above the 50 ng threshold.

In addition to the mono-nucleosome shift assay, binding was further assessed using a differential centrifugation assay (figure 4.1B). Briefly, condensate formation was induced via incubation with 4.5 mM $MgCl_2$, followed by incubation with 1:1 linker histone H1.0 per nucleosome. This was repeated with an Alexa-488 labeled H1.0, incubated with 601x12 arrays for either 1 hour, or overnight (ON). Arrays with and without the addition of H1.0 were also incubated at 0 mM Mg^{2+} for comparison. After a short centrifuge run, the pellet and supernatant were assessed through SDS-PAGE, with the expectation that H1 and nucleosome bands will show up in the pellet and not the supernatant if binding occurs under condensate forming conditions only. The high degree of self-association found in condensates makes them form structures so large

that they can easily be separated out from unassociated arrays or unbound proteins using differential centrifugation.

In figure 4.1B, under 4.5 mM $Mg2^{+}$, we see the presence of the nucleosome bands (3 bands around 10 to 15 kDa) appear in the pellet for the 601x12 arrays and not the supernatant. Similarly, with the addition of H1.0 and Alexa 488 H1.0, we see the nucleosome band plus the addition of the H1.0 band (27 kDa) apparent in the pellet fraction only and not the supernatant fractions. Differences in band densities suggest that Alexa 488 labeled H1.0 appears to have slightly less efficient binding to condensates than the unlabeled H1.0. Under 0 mM Mg^{2+}, the nucleosome bands for the 601x12 arrays appears in both the supernatant and the pellet fractions. This also is true with the addition of unlabeled H1.0 under the same conditions. The appearance of the H1.0 band in the pellet fractions only, and not in the supernatant, under 4.5 mM Mg^{2+} suggests that H1.0 indeed binds condensates. Under 0 mM Mg^{2+} H1.0 binding cannot be determined for this assay due to the indistinguishable supernatant and pellet fractions. However, it is important to note that the results support that self-associating properties of arrays at > 4 mM Mg^{2+} are responsible for differences found in the pellet and supernatant fractions. This is necessary to display that binding occurs to condensates alone, and that the differences between fractions are due to the self-interaction properties of nucleosome arrays at > 4 mM Mg^{2+}.

In Figure 4.1C we display the apparent binding of Alexa 488 labeled H1.0 condensates using fluorescence microscopy. Previous work has shown that in >4 mM Mg^{2+} fluorescently labeled 601x12 arrays appear as spherically induced globules, with an average radius of 200 nm (*59, 62*). In this assay, Alexa 488 labeled H1.0 was

incubated with both unlabeled arrays, as well as with Alexa 647 labeled arrays at a ratio of 0.5:1 H1.0 per nucleosome for 1 hour at 25°C before imaging. On the left-hand panel in figure 4.1D, we see the appearance of spherical globules in the green channel from labeled H1.0. While the appearance of H1.0 in apparent globules suggests it is bound to the unlabeled 601x12 condensates, we used the addition of Alexa 647 labeled 601x12 arrays to look for any overlap in red and green, which is more indicative of binding. In the right-hand panel, displaying red and green channels simultaneously, we see some overlap of Alexa 488 H1.0 and Alexa 647 H4 in the form of yellow spherical globules. This further supports apparent binding of H1.0 to the condensates.

4.22 Linker Histones Stabilize Condensate Self-Association Properties

It is well documented that H1 provides increased protection against MNase both *in vitro* using 5S rDNA, and with *Xenopus* oocytes *in situ* (*72, 73*). In particular, Belikov and colleagues looked at increasing ratios of H1, from 0 to 3 H1 per nucleosome in oocytes. They showed that with an increase in H1 ratio, there was an increase in DNA protection that plateaus around the ratio of 2:1 H1 per nucleosome (*73*). To test the ability of H1.0 to protect DNA from MNase digestion in 601x12 condensates, we looked at its behavior at a ratio of 1:1 and 2:1 H1 per nucleosome (see figure 4.2A). We digested the condensates using MNase in 5-minute intervals up to 20 minutes and 30 minutes for the ratio of 2:1 H1 per nucleosome. The fully intact 601x12 DNA appears as a band around 2500 bp on an agarose gel. As digestion proceeds, the 2500 bp band will fade and the bands for smaller DNA fragments will increase in apparent density. From figure 4.2A, we see that in the absence of H1.0, the 2500 bp band for 601x12 condensates disappears within 20 minutes. With a ratio of 1:1 H1.0 per nucleosome,

however, we see a gradual fading of the 2500 bp band up to 20 minutes without fully disappearing within this time frame, although digestion of smaller fragments does increase over this period. At a ratio of 2:1 H1.0 per nucleosome we see very strong apparent protection, with a bright 2500 bp fragment up to 30 minutes. This indicates that in the context of 601x12 condensates H1.0 provides protection from MNase digest, which is particularly pronounced at a higher ratio of H1 per nucleosome.

Strickfaden and Gibson showed that under varying conditions, chromatin can behave either like a solid or a liquid both *in vivo* and *in vitro* using 601x12 condensates *(62)*. Liquid promoting conditions for the condensates include a solution of Mg acetate, BSA, DTT, and glycerol, and solid promoting conditions with > 4 mM Mg^{2+} with low NaCl, EDTA and Tris (*62, 63*). We investigated the effect of H1.0 on the liquid and solid promoting conditions of the 601x12 condensates using the biochemical pelleting assay as well as fluorescence microscopy with Alexa 488 and Alexa 647 labeled arrays (see figure 4.2B, 4.2C). In the biochemical pelleting assay shown in figure 4.2B, we tested the 601x12 condensates under liquid promoting conditions in three ways. First, the condensates (601x12 arrays in 5 mM Mg^{2+}) with the addition of BSA alone; second, after short incubation of condensates with BSA, introducing a 1:1 ratio of H1.0 per nucleosome; and third, incubating a 1:1 ratio of H1.0 per nucleosome with condensates first, then adding the additional BSA (indicated in Figure 4.2B as *). We found that the addition of the BSA prevented 601x12 condensates from pelleting, indicating the promotion of liquid-like behavior of the condensates. This is evident by the presence of the 66 kDa band of BSA as well as the core histone bands present in both pellet and supernatant fractions. This was true even following the addition of H1.0 after BSA was

already present in solution. Notably, even under these conditions, H1.0 is present only in the pellet fractions and not the supernatant fractions. Interestingly, it appears that the order of introduction of either BSA or H1.0 matters for the ability of the 601x12 condensates to pellet. Under the conditions where H1.0 was added prior to the introduction of BSA, only BSA appeared in the supernatant fraction, with the core histones and the H1.0 band both absent from all supernatant fractions. This suggests that the presence of H1.0 prebound to the condensates provides additional stability, apparently maintaining the self-associative properties of the condensates themselves. Additionally, the later introduction of H1.0 may also provide some protection as well, as the core histone bands appear darker in the pellet fractions relative to supernatant than they do without the presence of H1.0 as well.

Finally, Strickfaden et al. observed that 601x12 condensates under the liquid promoting solution conditions behave as liquid by comparing red and green labeled condensates using fluorescent microscopy (*62*). Under liquid promoting solution conditions (150 mM K Acetate, 1 mM Mg Acetate, BSA, DTT and glycerol) the condensates would merge to form larger apparent yellow droplets from the overlapping red and green labeled arrays. Strickfaden showed that this did not occur under the > 4 mM Mg^{2+} conditions used to form the 601x12 condensates (*62*). We wanted to see how the addition of H1.0 affected the apparent “liquid” promoting behavior of the condensates under the same conditions. We did so by adding a ratio of 2:1 H1.0 per nucleosome to the 601x12 arrays, and then allowing it to bind for 30 minutes at 25°C before the introduction to the liquid promoting solution. In figure 4.2C, we show that the presence of H1.0 bound to the condensates prevents the apparent blending of red and

green condensates. This is shown in figure 4.3C immediately after mixing, from 0 min up to 90 minutes after mixing. This suggests that the presence of H1.0 in the condensates promotes their structural stability, promoting a solid-like state for the condensates.

4.23 *In vitro* Condensates Show Accessibility to Proteins of Varying Size Without Disrupting Condensate Structure

The condensate environment is composed of interdigitated 10-nm fibers, facilitated by the self-interaction of the nucleosome tails (*4*). We show in figure 4.1 that this environment is accessible to binding by linker histones, which are known to interact with both nucleosomes and linker DNA. We asked if the condensate environment would further be accessible to additional chromatin binding proteins and larger protein complexes without disrupting the structure and self-association properties of the condensate itself. We tested this using two proteins with distinct binding preferences on chromatin: Sirtuin 6 (SirT6) and Polymerase epsilon (Pol ε). SirT6 is a 39 kDa heterochromatin binding protein with important functions in promoting chromatin structural stability, DNA repair, as well as NAD^+ dependent deacetylase activity(*74*). As a dimer, SirT6 interacts with the acidic patches found on the H2A/H2B dimers within the nucleosome (*75*). Pol ε is involved in chromosomal replication and binds single stranded and double stranded DNA (*76*). Pol ε is a holoenzyme composed of four subunits; dpb2 (78 kDa), dpb3 (23 kDa), dpb4(22 kDa), and Pol 2 (255 kDa) (*76*).

First, using the biochemical pelleting assay, we assessed if SirT6 and Pol ε could bind condensates (figure 4.3 A, 4.3B). SirT6 was incubated with condensates from a ratio of 0.5 up to 2.5 SirT6 per nucleosome (figure 4.3A). We found that up to this ratio

we found SirT6 is present in the pellet fractions, with no detectable amounts found in the supernatant fractions (see Appendix Figure 4.2). Similarly, we saw that Pol ε incubated with condensates in ratios of 0.16 and 1.0 Pol ε per nucleosome showed no detectable amounts in the supernatant fractions (figure 4.3B). This indicates that both SirT6 and Pol ε are likely binding nucleosomes and DNA, respectively, found in the condensate environment.

Additionally, we looked at the morphological effects on condensates upon binding by both SirT6 and Pol ε using fluorescence microscopy. We incubated a 2:1 ratio of SirT6 per nucleosome with Alexa 488 labeled 601x12 condensates (5 mM Mg^{2+}). In figure 4.3C we show that condensates bound with 2:1 ratio of SirT6 per nucleosome show little difference in both size and shape from condensates composed only of DNA and nucleosomes (null condensates) (*59*). Similarly, we incubated an LD 655 labeled Pol ε with the Alexa 488 labeled 601x12 condensates at a ratio of 1:6 Pol ε per nucleosome. In Figure 4.3D, overlaid green and red channels show the presence of apparently yellow condensates. This overlap between the labeled Pol ε and the 601x12 condensed arrays lends support to the ability of Pol ε to bind 601x12 condensates. In addition, these Pol ε bound condensates show little variability from the null condensates in size and shape. It seems that both SirT6 and Pol ε are not only able to bind nucleosomes and DNA within condensates, but they can do so without effecting the apparent structure of the condensates themselves. This suggests that both SirT6 and Pol ε can bind without disrupting the self-association properties between nucleosomes within condensates.

4.24 Linker Histones Partially Restrict Binding of Polymerase ε and SirT6

It is a long-held assumption that for certain proteins to bind condensed chromatin, it is first required to release linker histones to both decompactify and provide access to binding sites (*35, 36, 77*). It is possible that linker histones may limit binding by sterically blocking access to either nucleosomes, or adjacent linker DNA. We therefore asked the question if chromosomal proteins and protein complexes can also access and bind condensates either in the presence or absence of H1.

We used the biochemical pelleting assay to determine whether the presence of H1.0 pre-bound within condensates prevents access to nucleosome binding by SirT6. We incubated a 1:1 ratio of H1.0 per nucleosome (H1/N) with condensates before the addition of a 4:1 ratio of SirT6. Additionally, we also incubated condensates with a saturated excess, or 4:1 H1/N before the addition of a 2:1 ratio of SirT6/N (see figure 4.3A). We found that the presence of H1.0 at 1:1 ratio per nucleosome did not prevent the binding of SirT6, with no detectable amount of SirT6 present in the supernatant fractions. However, at a ratio of 4:1 H1.0/N, we did see some exclusion of SirT6 with a faint amount detected in the supernatant fraction (figure 4.3A). While the presence of 1:1 H1.0/N did not prevent the binding of SirT6, higher ratios did appear to partially restrict additional binding to nucleosomes. The higher ratios of H1.0 and SirT6 also appeared to influence the morphology of the condensates as well. In figure 4.3C, we see that Alexa 488 labeled condensates in the presence of both 2:1 H1.0 and 2:1 SirT6 per nucleosome caused the condensates to appear to form more complex structures, including dimers. The additional presence of H1.0 at a higher ratio appears to influence

not only the binding ability of SirT6 but also effect the apparent structure of the condensates themselves.

We further investigated if the presence of H1.0 would prevent access to binding to the linker DNA between nucleosomes by the holoenzyme Pol ε. First, we introduced 1:1 H1.0/N to the condensates. Next, we incubated increasing ratios of Pol ε, including 0.5, 0.75 and 1:1 per nucleosome to condensates with pre-bound H1.0. Following the biochemical pelleting assay, we found that the presence of 1:1 H1.0/N did not prevent binding of Pol ε to the condensates at a ratio of 0.5 Pol ε/N (see figure 4.3B). Interestingly, at a 0.75 and 1:1 ratio of Pol ε introduced, we find apparent signs of unbound or excess present in the supernatant fraction. In figure 4.3B we also see that in the absence of H1.0, introducing 1:1 Pol ε/N presents no excess or unbound amounts detectable in the supernatant. This indicates that the presence of H1.0 likely partially restricts binding access of linker DNA to Pol ε.

4.25 Condensates Provide Additional Binding Sites for Linker Histones beyond the Nucleosome

Recent studies have shown that within complex condensed chromatin there are multiple distinct binding modes that can be adopted in addition to the known on-dyad nucleosome binding mode (*45*). Interestingly, it was recently shown that there may be unique differences in binding modes found among variants H1.0 and H1x (see Appendix Figure 5). Here, we used the biochemical pelleting assay to determine if different linker histone variants can bind condensates above a 1:1 H1/N, and probe any differences between variants. We investigated the binding of variants H1.1 to H1.5 by titrating condensates with input ratios (r^{H1}) of H1/N varying from 0, .25, .50, .75, 1.0, 1.5, 2, 2.5,

3, 3.5, 4, 4.5, 5, 5.5, and 6. To quantitate the ratio of linker histone per nucleosome found within the pellet fractions using SDS PAGE, we co-loaded in-gel standards of known amounts (in ug) of linker histone. These standards were then used to generate a standard curve, from which we could use to calculate the amounts in ug of histones and core histones (see figure 4.4). From the amount in ug calculated, we then calculate the amounts of histones in moles, and convert moles to mole ratios H1/nucleosome (tables 4.1-5).

Importantly, we show that all variants tested did have a detectable amount of bound linker histone in pellets higher than 1:1 H1/N (figure 4.4). This suggests that within the condensate environment, linker histones H1.1 to H1.5 can bind additional targets beyond expected nucleosome binding sites. We found that up to an r^{H1} of 6, linker histones H1.3, H1.4 and H1.5 appear to saturate condensates around a ratio of 2.5 (see figure 4.4). The linker histone H1.5 has an upward trend suggestive of saturation upon even higher r^{H1}, however it is important to note that r^{H1} of 5.5 and 6 have statistically overlapping ranges. Therefore, this apparently increasing trending we see with H1.5 may be superficial. Interestingly, H1.1 and H1.2 show significant variation from H1.3, H1.4 and H1.5. In figure 4.4A, we can see that H1.1 and H1.2 appear to bind and saturate condensates from ratios between 3 and 4 H1/N. Along with the apparent higher binding, there are also much higher standard deviations than were seen with the other variants tested found at the higher r^{H1}. H1.1 and H1.2 therefore show an apparent variant specific difference in binding to the 601x12 condensates from H1.3, H1.4 and H1.5.

4.26 Linker Histones Facilitate Complex Chromatin Fiber Contacts *in vitro*

We showed that linker histones H1.1, H1.3, H1.4 and H1.5 can bind condensates above a ratio of 1:1 H1/N. As such, we investigated the effect of the higher binding ratios of linker histones on condensate morphology. Recent studies have shown that H1 displays chromatin fiber cross-linking abilities that are enhanced at ratios above 1:1 of H1/N (*45*). Therefore, we investigated the effect of r^{H1} on the apparent condensate morphology, specifically looking at input ratios of 0.5, 1, 2.0 and 4.0 (see figure 4.5). In figure 4.5, we show that isoforms H1.1, H1.3, H1.4 and H1.5 show a greater propensity to form condensate to condensate contacts at higher r^{H1}. Below r^{H1} of 1:1 H1/N, condensates mostly appear spherical in shape, averaging between 200 and 300 nm (see Appendix Table 2). With increasing r^{H1} we see the assembly of complex aggregates composed of multiple linked condensates (figure 4.5). These structures appear to form twisted chains, whose links are made up of the smaller 200-300 nm condensates. Importantly, we do not see the formation of these complex structures in the absence of H1, nor does increasing the concentration of 601x12 arrays does not appear to facilitate the formation of these structures (*59, 62*). All variants we analyzed show an increasingly pronounced aggregate forming activity beginning at an r^{H1} of 1:1 H1/N and above. At the 2:1 ratio and above, the mean effective radius, or the longest length across for both linked and unlinked condensates measured in nm, shifts from 260 nm in the absence of H1 to between 380-400 nm for all variants tested (see Appendix Table 2 and Appendix Figure 6). Therefore, we show that linker histones facilitate the self-association of condensates *in vitro.*

4.3 Discussion

4.31 Linker Histones Find Additional Binding Sites in Condensates

Linker histones readily bind condensates above a 1:1 ratio of LH/N. Most structural work with linker histones has been done with mono- and tri-nucleosomes where a 1:1 ratio between histone and nucleosome was assumed, and linker histones were observed binding the dyad axis of the nucleosome (*36, 44, 71, 78, 79*). Recently, linker histones were shown to display additional binding modes when present in complex chromatin fibers, and may exceed the 1:1 ratio of linker LH/N traditionally assumed (*45*). X-ray crystallography has shown that linker H1.0 exhibits an off-dyad mode of binding that physically cross-links dinucleosomes into fibers (*45*). The non-dyad binding modes suggest there may be variability in how the linker histones can bind and interact with the chromatin environment. This suggests that H1 may be capable of efficiently penetrating chromatin fibers to find additional binding sites, allowing for binding above the assumed 1:1 ratio. Additional binding by H1 may serve to strengthen intermolecular contacts between nucleosomes, further stabilizing chromatin compaction (*71*). Indeed, in live cells, it has been observed that increasing density of linker histone positively correlates to heterochromatin and heterochromatin markers (*36*).

4.32 Condensates Serve as Effective Models for Chromatin Domains

The local density of linker histones within chromatin domains appears to play a critical role in compartment regulation within chromatin (*52*). Higher order structures called domains of approximately 200 nm were observed through both light and electron microscopy (*64, 80, 81*). Hi-C data and super resolution imaging shows eukaryotic genomes are organized into large topologically associated domains (TADs) as well as

smaller contact/loop domains (*82, 83*). TADs can further be divided into distinct “A” and “B” compartments, where A compartments may be more transcriptionally active euchromatin, and B is likely inactive and repressive heterochromatin (*52, 54*). Using Hi-C, Wilcockson et al. showed higher than average levels of linker histone were present in B compartments as well as A compartments containing repressive PRC2 (*52*). Further, Wilcockson et al. found that a reduction in H1 stoichiometry shifted the more repressive B type compartments to more active A compartments (*52*). However, the Hi-C data gives no direct structural information.

The condensates serve as good models for the 200 nm domains seen *in vivo*. We show that at higher stoichiometries, linker histones promote further self-association between condensates through increasing fiber-fiber contacts. Here, linker histones may serve a role in compartment maintenance by globally stabilizing chromatin fibers. Linker histones stabilize chromatin by promoting increased fiber-fiber contacts at high stoichiometries. The increased stability and condensation of linker histone rich regions contributes to the self-organization of interphase chromosomes. It is probable that the effect of linker histones in stabilizing chromatin compartments is only modestly structurally repressive, and that repression is driven more by additional protein-protein interactions. For example, higher levels of linker histone may serve to promote the activity and recruitment of methyltransferases (*35*). H1 bound recombinant dinucleosomes displayed methylation of H3K9 by Suv39h1 and SETDB1 at significantly higher levels than in the absence of H1 (*35*). Additional studies have shown that H1 interacts with additional proteins such as SETDB1 while simultaneously bound to the nucleosome using its CTD (*35*). It is also possible that variant specific differences

between linker histones may play an additional role in mediating a domain-domain interaction as well as promoting further protein-protein interaction.

4.33 Linker Histones Show Variant Specific Differences in Binding Condensates

H1 structure consists of a highly evolutionarily conserved globular domain, with more variable N-terminal and C-terminal domains (*7*). The globular domain binding facilitates the protection of ~20 base pairs of linker DNA (*7*). The other domains are likely more important for the formation of higher order chromatin structures. The N-terminal domain (NTD) is nominally unstructured, hydrophobically enriched, and likely plays a role in binding the nucleosome itself, and deletion of the NTD from H1 has shown reduced binding affinity for nucleosomes (*7*). The C-terminal domain (CTD) is intrinsically disordered, has a net positive charge, and accounts for more than half of linker histones' sequence (*7*). There is no overall CTD sequence conservation among H1's isoforms, however ~40% share evenly distributed positively charged residues (*41*). The CTD is likely involved in the formation, and stabilization, of linker DNA into higher order structures (*36, 41, 71, 84*). NMR spectroscopy has shown that H1 displays dynamic, almost liquid like behavior in chromatin domains (*40*). This action may be facilitated by its unstructured C-terminal tail. The length, charge, and posttranslational modification sites vary among isoforms, suggesting distinct roles in chromatin structure regulation (*7, 36, 71, 84*).

Apparent variant specific differences were found in the binding saturation of condensates by H1.1 and H1.2. Variants H1.3, H1.4, and H1.5 all appear to bind condensates between a maximum observed ratio of 2-3 H1/N up to r^{H1} of 6. Under the same conditions, however, we observed H1.1 and H1.2 bind a maximum of 3-4 H1/N

with much more variability shown by H1.1 at high r^{H1} (Figure 4.4). Observed binding differences may be due to the CTD on isoforms. Th'ng et al. classified histone variants into broad binding groups based on FRAP experiments with GFP fusion proteins(*85*). Affinities were linked to apparent mobilities, with high mobility group, including H1.1 and H1.2 having the lowest affinities, and the lowest mobility group including H1.4 and H1.5 having the highest affinities (*2*). Indeed, H1.1 and H1.2 have the shortest C-terminal tails of the somatic variants, showing the lowest density of positive charge, while H1.4 and H1.5 have the longest C-terminal tails (*86*). The CTD on linker histones is essential to their mobility within chromatin and is likely responsible for additional binding modes observed. Stasevich et al. showed that the C-terminal tails on linker histone H1.0 likely bind to linker DNA nonspecifically first, followed by more stable binding to along nucleosome sites (*87*).

The electrostatic contributions of the linker histones themselves appears important to maintaining condensate stability. In Appendix figure 4.3, we show that the presence of 200 mM NaCl in solution causes the condensates to fall apart, where nucleosome bands appear in both pellet and supernatant fractions. However, with the addition of linker histones H1.0 and H1.5, there is additional protection against falling apart up to 300 mM NaCl. Between H1.0 and H1.5, H1.5 does not make any marked appearance in supernatant fractions until above 350 mM, while H1.0 appears in the supernatant clearly around 300 mM (see Appendix Figure 3). This difference may be due to the longer, highly positively charged CTD on H1.5 relative to H1.0, causing it to have a higher apparent binding affinity to condensates. Therefore, it is reasonable to assume that the variability we observe with H1.1 may be due to a higher degree of

promiscuity through a shorter CTD, and lower overall binding affinity to chromatin, making it more apparently dynamic than variants H1.3, H1.4 and H1.5. It is possible that variant specific differences may be important for how linker histones regulate the chromatin architecture, and landscape. Linker histones may do this, as Gibbs and Kriwacki have suggested, by acting as a type of “electrostatic glue” through non-specific interactions between its CTD and linker DNA (*40*).

4.34 Linker Histone Bound Condensates Remain Accessible to Additional Proteins

Condensates formed from the self-association of 601x 12 bp arrays serve as an *in vitro* model for chromatin structure and behavior. Condensates show the same packaging and physical state of chromatin fiber in live cells (*4, 59, 62*). However, it was unknown whether these condensates were also accessible to chromatin binding proteins of varying size, nor the effect on apparent condensate stability and morphology. Here, we show that these condensates appear accessible to binding by linker histones, SirT6, as well as larger holoenzymes of 378 kDa such as Pol ε (Figure 4.3). Importantly, binding by Pol ε is possible without disrupting the large-scale condensed structure of the condensates themselves (Figure 4.3D). We show that while the presence of bound H1.0 alone is not enough to prevent binding of Pol ε, it does appear to limit binding to some degree (Figure 4.3B). Additionally, bound linker histones show stabilizing effects on condensates, not only by limiting access to nuclease digestion, but also by promoting self-association properties of condensates (Figure 4.2). The presence of BSA causes condensates to dissociate. BSA is often used as a blocking agent to prevent non-specific binding (*88*). Because histone tail interactions are weak and transient, this may cause competition between BSA and the adjacent

nucleosome-nucleosome interactions. The presence of linker histones, however, appears to further stabilize condensates by preventing their dissociation when BSA is introduced to solution.

Linker histones appear vital to the organization of TADs into compartment types. In condensates, linker histones both facilitate and stabilize fiber-fiber contacts. This stabilization effect may play an important role in the organization of domains through a type of phase separation. The condensation effect on chromatin by linker histones alone does not make the landscape completely inaccessible to binding by additional proteins. In fact, linker histones themselves are likely dynamically diffusing within chromatin domains while simultaneously stabilizing chromatin through the dynamic cross-linking of adjacent fibers. The stabilized condensed chromatin then likely aids in the physical organization of higher order chromatin domains as well as in the recruitment of relevant protein partners by acting as a type of scaffolding.

4.4 Figures

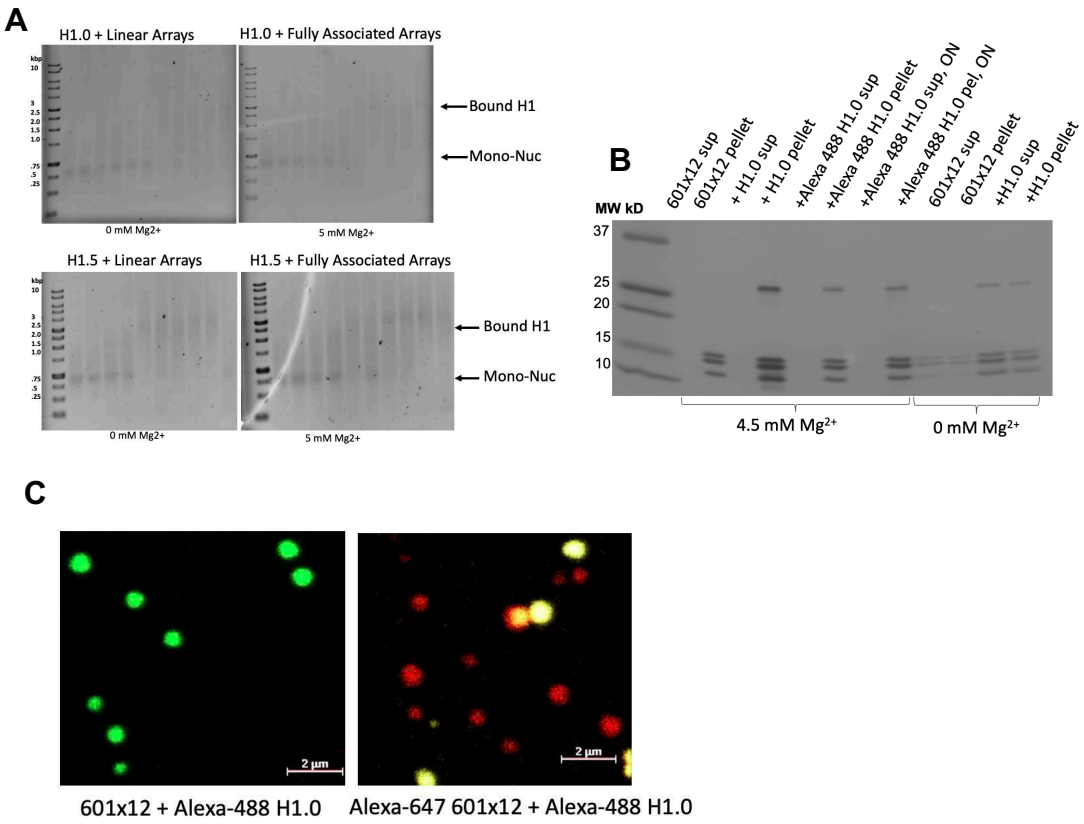

Figure 4.1: Linker Histones Bind Nucleosomes in Linear Arrays and Condensates. A: Histone H1.0 and H1.5 were titrated from 0 to 100 ng into 600 ng 601x12 arrays in either 0 or 5 mM Mg^{2+} ,and incubated for 30 minutes before digestion with EcoRI. H1 binding is evident by the appearance of a band shift from 500 to 1000- 2500 kbp. Goldbio 1kb DNA ladder shown for reference. **B:** Biochemical Pelleting assay on SDS PAGE. H1.0 appears as a band around 27 kD, and the core histones representing the nucleosome as 3 bands from 10 to 15 kD. Biorad Precision Plus All Blue Standards protein ladder shown for reference. **C:** Fluorescence microscopy binding assay, 2 um inset. Lefthand panel displays Alexa-488 H1.0 incubated with unlabeled 601x12 arrays at 5 mM Mg^{2+}. Righthand panel includes Alexa-647 arrays and Alexa-488 H1.0 with overlapping red and green channel, 5 mM Mg^{2+}.

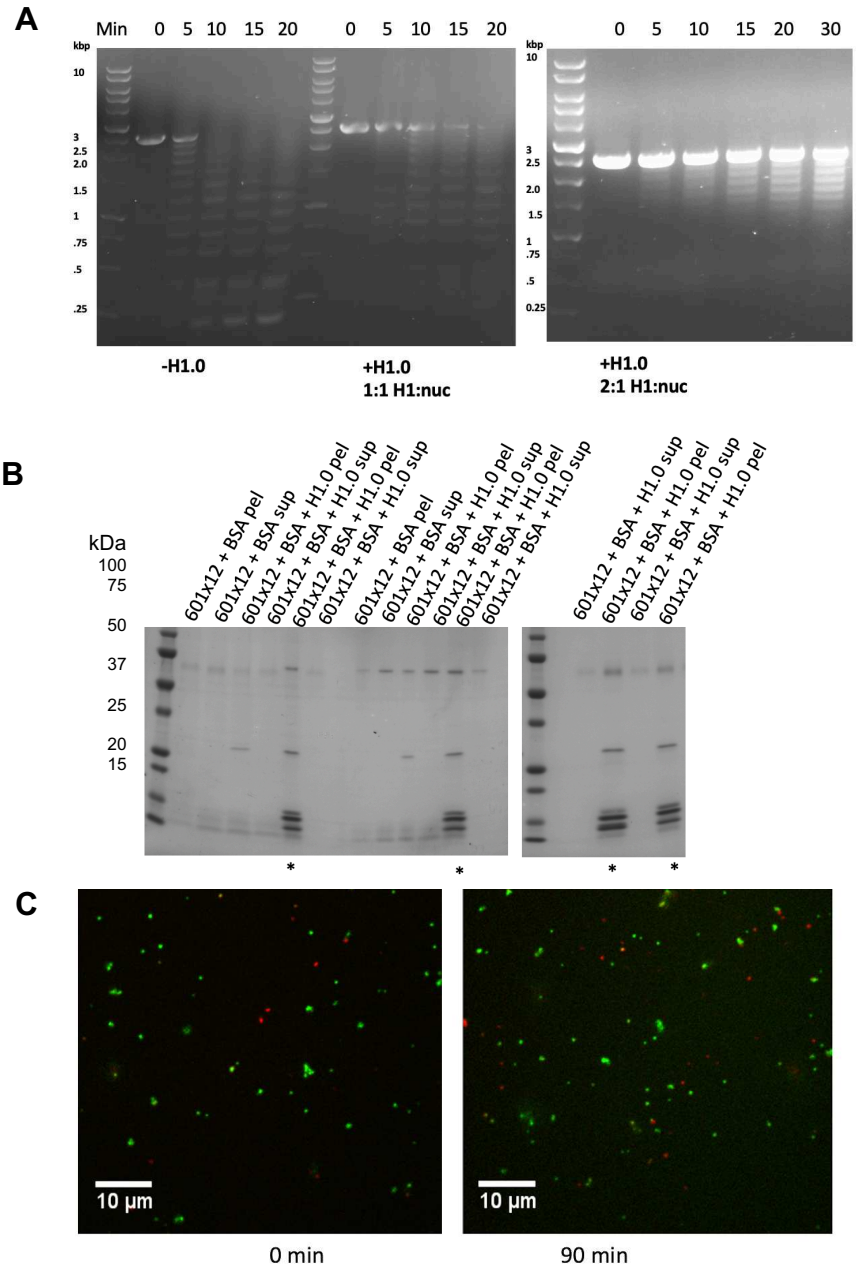

Figure 4.2: Linker Histones Stabilize Condensate Self-Association Properties. A: MNase digest on 601x12 condensates with and without the addition of H1.0. Time intervals of 5 to 20 minutes (30 min for 2:1 H1.0/N reaction) were taken by removing a small fixed amount from the reaction mixture and quenching with EDTA and ice. Undigested DNA is appears as a band around 2500 bp representing the full 601x12 template. Goldbio 1kb DNA ladder shown for reference. **B:** Biochemical pelleting assay done with the addition of BSA and H1.0. BSA was added to the condensates prior to the introduction of H1.0 in all cases except those indicated with (*). In (*) reactions, H1.0 was added to condensates before the addition of BSA. The BSA band appears around 66 kDa, H1.0 around 27 kDa, and core histones between 10 and 15 kDa. Biorad Precision Plus All Blue Standards protein ladder shown for reference.**C:** Fluorescence microscopy, 10 um inset, on Alexa 488 labeled 601x12 arrays and Alexa 647 labeled 601x12 arrays bound with H1.0 in 150 mM K acetate, 1 mM Mg acetate, BSA, DTT, and glycerol. Imaged immediately after mixing (0 min) and 90 minutes after mixing.

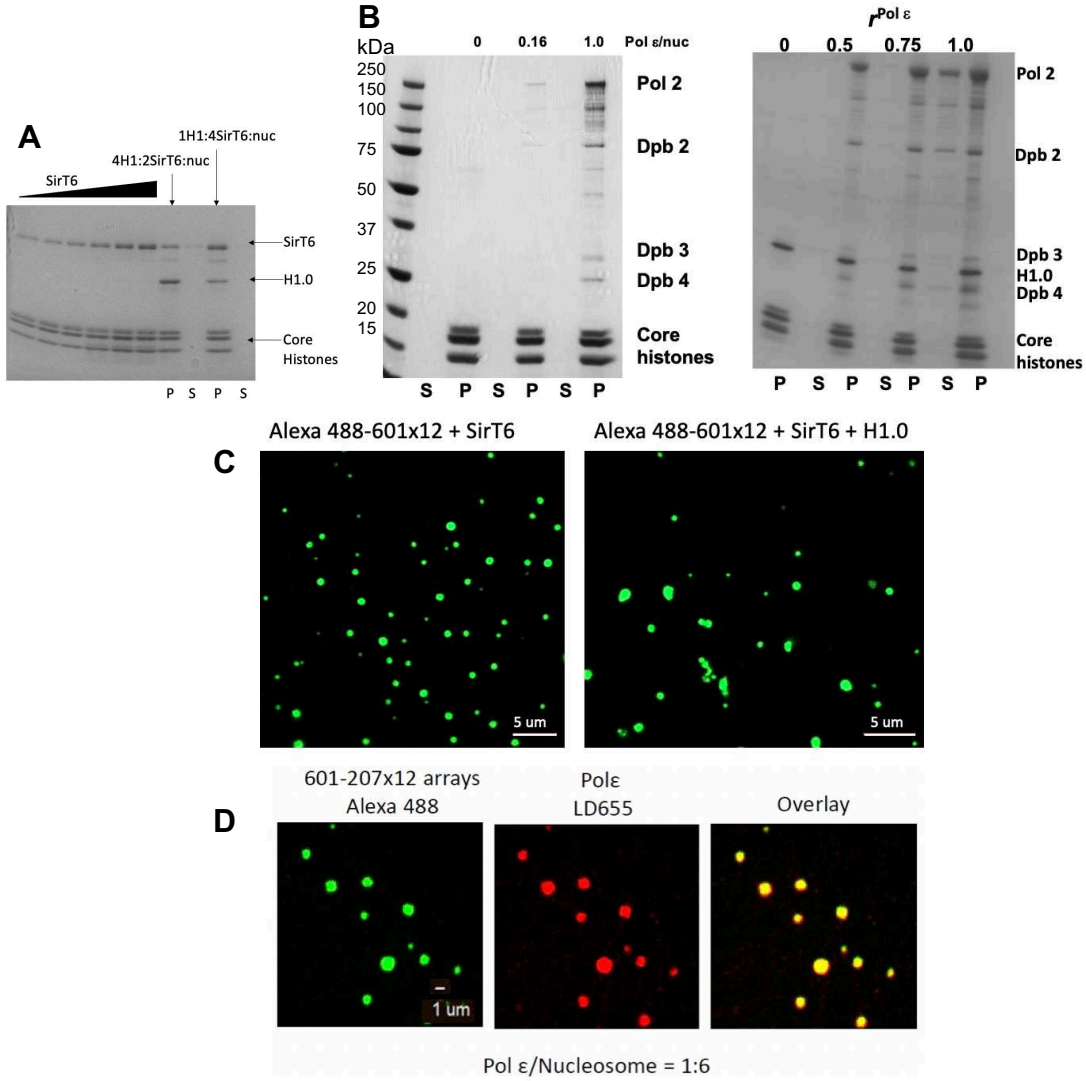

Figure 4.3: *In vitro* Condensates Show Accessibility to Proteins of Varying Size Without Disrupting Condensate Structure. A: Biochemical Pelleting Assay with 601x12 condensates and SirT6 and H1.0. From left to right SDS PAGE loaded with pellets from binding assay including increasing ratios of SirT6 per nucleosome from 0.5, 0.75, 1, 1.5, 2, 2.5. Immediately following shows pellets (P) and supernatant (S) from binding assay in the presence of excess H1.0 (4:1 H1/N) and stoichiometric SirT6 (2:1 SirT6/N), and stoichiometric H1.0 (1:1 H1.0/N) and excess SirT6 (4:1 SirT6/N). SirT6 appears as a band around 42 kDa. **B:** Biochemical Pelleting Assay with holoenzyme polymerase ee and 601x12 condensates in the absence (left) and presence (right) of pre-bound H1.0. Pellets marked as (P), supernatant demarked as (S). Biorad Precision Plus All Blue Standards protein ladder shown for reference. **C:** Lefthand panel shows Alexa 488 labeled 601x12 arrays in 5 mM Mg^{2+} mixed with 2:1 ratio of SirT6 per nucleosome. Righthand panel shows Alexa 488 labeled 601x12 arrays in 5 mM Mg^{2+} with the addition of 2:1 SirT6/N and 1:1 H1.0/N. **D:** Alexa 488 labeled condensates with LD-655 labeled Pol ε. Left panel shows the 488 channel labeled 601x12 condensates. The center panel shows 647 channel with LD-655 labeled Pol ε. Right panel shows the overlap of both channels.

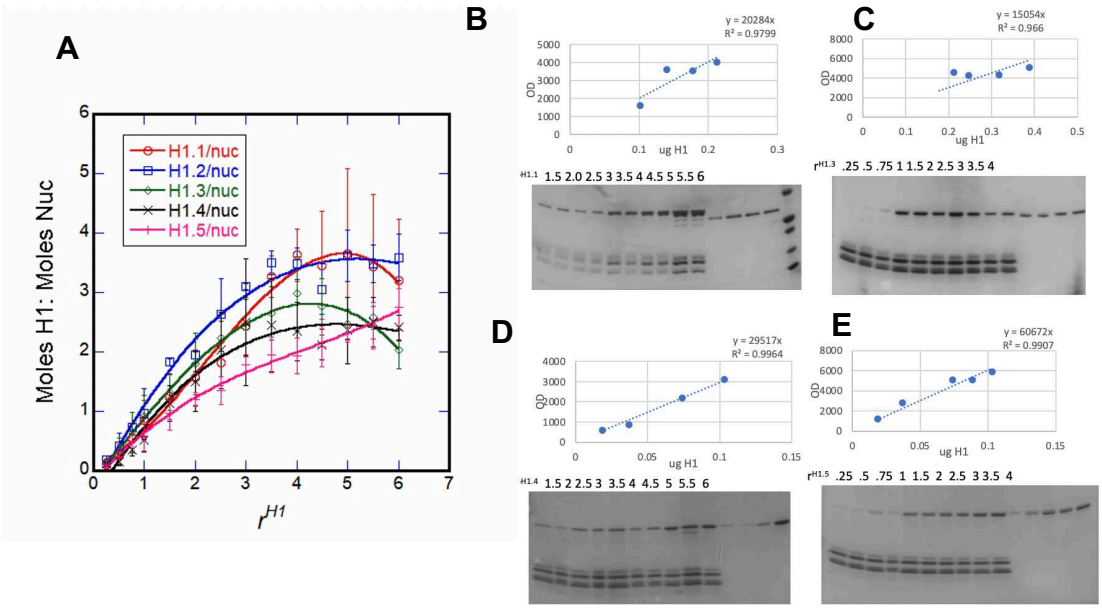

Figure 4.4: Condensates Provide Additional Binding Sites for Linker Histones beyond the Nucleosome. A: Binding Plots for linker histones were generated by analyzing mole ratios of linker histone to core histones in the pellet fraction from the biochemical pelleting assay. The horizontal axis represents the input mole ratio of linker histone per nucleosome. The vertical axis represents the measured amount of H1 per nucleosome (H1/N) found in the pellet fractions. Band intensities were measured using ImageJ, and converted to ug H1 using in-gel standards and a standard plot. **B:** A representative gel from H1.1 is shown with its standard plot above. Standards shown for H1.1 include .101 ug, .140 ug, .178 ug and .212 ug. Biorad Precision Plus All Blue Standards protein ladder shown for reference. **C:** A representative gel from H1.3 is shown with its standard plot above. Standards for H1.3 are .212 ug, .245 ug, .317 ug, and .390 ug. **D:** Representative gel from H1.4 is shown with its standard plot above. Standards for H1.4 include .0185 ug, .037 ug, .074 ug, and .103 ug. **E:** A representative gel from H1.5 is shown with its standard plot above. Standards loaded for H1.5 include .0185 ug, .037 ug, .074 ug, .089 ug and .103 ug.

Table 4.1: r^{H1} are input ratios (H1.1/N). Amounts of H1.1 were calculated using a standard curve for each gel

$r^{H1.1}$	Moles H1.1	Moles Nuc	H1.1/Nuc
0.25	$3\pm2\times10^{-13}$	$3\pm1\times10^{-12}$	0.1±0.1
0.5	$1.0\pm0.6\times10^{-12}$	$3.7\pm0.5\times10^{-12}$	0.3±0.2
0.75	$2\pm1\times10^{-12}$	$4\pm1\times10^{-12}$	0.6±0.2
1	$3\pm2\times10^{-12}$	$4\pm1\times10^{-12}$	0.8±0.3
1.5	$5\pm2\times10^{-12}$	$3.9\pm0.8\times10^{-12}$	1.2±0.4
2	$6\pm5\times10^{-12}$	$4\pm2\times10^{-12}$	1.6±0.5
2.5	$4\pm3\times10^{-12}$	$2\pm1\times10^{-12}$	1.8±0.4
3	$7\pm2\times10^{-12}$	$3\pm1\times10^{-12}$	2.4±0.5
3.5	$7\pm5\times10^{-12}$	$2\pm1\times10^{-12}$	3.3±0.3
4	$1.1\pm0.5\times10^{-11}$	$3\pm2\times10^{-12}$	3.6±0.4
4.5	$9\pm2\times10^{-12}$	$3\pm1\times10^{-12}$	3.4±0.9
5	$1.1\pm0.3\times10^{-11}$	$3\pm1\times10^{-12}$	4±1
5.5	$1.2\pm0.4\times10^{-11}$	$4\pm1\times10^{-12}$	3±1
6	$1.3\pm0.5\times10^{-11}$	$3.9\pm0.6\times10^{-12}$	3±1

Table 4.2: r^{H1} are input ratios (H1.3/N). Amounts of H1.3 were calculated using a standard curve for each gel

$r^{H1.3}$	Moles H1.3	Moles Nuc	H1.3/Nuc
0.25	$4\pm2\times10^{-13}$	$4\pm3\times10^{-12}$	0.13±0.06
0.5	$8\pm7\times10^{-13}$	$2.4\pm0.7\times10^{-12}$	0.3±0.2
0.75	$3\pm2\times10^{-12}$	$5\pm3\times10^{-12}$	0.6±0.3
1	$3\pm2\times10^{-12}$	$3\pm2\times10^{-12}$	0.9±0.3
1.5	$2.9\pm0.6\times10^{-12}$	$2.2\pm0.3\times10^{-12}$	1.3±0.3
2	$4\pm2\times10^{-12}$	$2.1\pm0.8\times10^{-12}$	1.8±0.5
2.5	$4.3\pm0.3\times10^{-12}$	$1.9\pm0.3\times10^{-12}$	2.2±0.3
3	$5\pm2\times10^{-12}$	$2.1\pm0.5\times10^{-12}$	2.4±0.5
3.5	$4\pm1\times10^{-12}$	$2.1\pm0.4\times10^{-12}$	2.6±0.4
4	$6.7\pm0.4\times10^{-12}$	$2.3\pm0.5\times10^{-12}$	3.0±0.6
4.5	$9\pm8\times10^{-12}$	$4\pm3\times10^{-12}$	2.8±0.5
5	$1.5\pm0.7\times10^{-11}$	$6\pm3\times10^{-12}$	2.5±0.3
5.5	$1\pm1\times10^{-11}$	$6\pm4\times10^{-12}$	2.6±0.2
6	$8\pm8\times10^{-11}$	$5\pm5\times10^{-12}$	2.0±0.3

Table 4.3: $r^{H1}$are input ratios (H1.4/N). Amounts of H1.4 were calculated using a standard curve for each gel

$r^{H1.4}$	Moles H1.4	Moles Nuc	H1.4/Nuc
0.25	$7\pm8\times10^{-13}$	$6\pm1\times10^{-12}$	0.11±0.03
0.5	$8\pm6\times10^{-13}$	$6\pm6\times10^{-12}$	0.15±0.06
0.75	$2\pm1\times10^{-12}$	$6\pm7\times10^{-12}$	0.4±0.1
1	$2\pm2\times10^{-12}$	$6\pm7\times10^{-12}$	0.5±0.2
1.5	$2\pm1\times10^{-12}$	$2\pm1\times10^{-12}$	1.1±0.3
2	$8\pm7\times10^{-12}$	$6.7\pm0.9\times10^{-12}$	1.4±0.5
2.5	$9\pm7\times10^{-12}$	$6\pm8\times10^{-12}$	1.7±0.6
3	$9\pm9\times10^{-12}$	$5\pm7\times10^{-12}$	2±1
3.5	$1\pm1\times10^{-11}$	$5\pm7\times10^{-12}$	2.1±0.8
4	$1\pm1\times10^{-11}$	$5\pm6\times10^{-12}$	2.2±0.5
4.5	$6\pm0.8\times10^{-12}$	$3.0\pm0.7\times10^{-12}$	2.1±0.3
5	$7\pm3\times10^{-12}$	$2.8\pm0.6\times10^{-12}$	2.6±0.6
5.5	$7\pm3\times10^{-11}$	$3\pm1\times10^{-12}$	2.3±0.4
6	$7\pm2\times10^{-11}$	$3.1\pm0.6\times10^{-12}$	2.4±0.2

Table 4.4: r^{H1} shows input ratios (H1.5/N). Amounts of H1.5 were calculated using a standard curve for each gel

$r^{H1.5}$	Moles H1.5	Moles Nuc	H1.5/Nuc
0.25	$1.8\pm0.9\times10^{-13}$	$1.6\pm0.5\times10^{-12}$	0.10±0.03
0.5	$5\pm3\times10^{-13}$	$2.0\pm0.2\times10^{-12}$	0.2±0.1
0.75	$1.0\pm0.2\times10^{-12}$	$2.0\pm0.1\times10^{-12}$	0.5±0.1
1	$1.1\pm0.6\times10^{-12}$	$1.8\pm0.4\times10^{-12}$	0.6±0.2
1.5	$1.6\pm0.5\times10^{-12}$	$1.74\pm0.04\times10^{-12}$	1.0±0.3
2	$2.0\pm0.2\times10^{-12}$	$1.9\pm0.1\times10^{-12}$	1.2±0.1
2.5	$1.7\pm0.5\times10^{-12}$	$1.9\pm0.1\times10^{-12}$	1.3±0.2
3	$3.4\pm0.4\times10^{-12}$	$1.9\pm0.2\times10^{-12}$	1.8±0.1
3.5	$2.2\pm0.5\times10^{-12}$	$1.8\pm0.1\times10^{-12}$	1.9±0.3
4	$3.7\pm0.7\times10^{-12}$	$2.1\pm0.2\times10^{-12}$	1.9±0.3
4.5	$5\pm1\times10^{-12}$	$2.4\pm0.3\times10^{-12}$	2.1±0.3
5	$5.3\pm0.7\times10^{-12}$	$2.3\pm0.3\times10^{-12}$	2.3±0.1
5.5	$5.7\pm0.8\times10^{-12}$	$2.3\pm0.2\times10^{-12}$	2.4±0.4
6	$6\pm1\times10^{-12}$	$6\pm0.3\times10^{-12}$	2.7±0.3

Table 4.5: $r^{H1}$are input ratios (H1.2/N). Amounts of H1.4 were calculated using a standard curve for each gel

$r^{H1.2}$	Moles H1.2	Moles Nuc	H1.2/Nuc
0.25	$3\pm1\times10^{-13}$	$1.9\pm0.8\times10^{-12}$	0.18±0.08
0.5	$1.0\pm0.7\times10^{-12}$	$2.6\pm0.6\times10^{-12}$	0.4±0.2
0.75	$2\pm1\times10^{-12}$	$3\pm1\times10^{-12}$	0.7±0.2
1	$2\pm1\times10^{-12}$	$2.4\pm0.5\times10^{-12}$	1.0±0.4
1.5	$5\pm1\times10^{-12}$	$2.6\pm0.7\times10^{-12}$	1.83±0.06
2	$5\pm2\times10^{-12}$	$2.8\pm0.8\times10^{-12}$	1.9±0.3
2.5	$7\pm4\times10^{-12}$	$2\pm1\times10^{-12}$	2.6±0.6
3	$9\pm1\times10^{-12}$	$2.8\pm0.4\times10^{-12}$	3.10±0.05
3.5	$1.03\pm0.08\times10^{-11}$	$3.0\pm0.3\times10^{-12}$	3.5±0.2
4	$9\pm3\times10^{-11}$	$2.5\pm0.8\times10^{-12}$	3.5±0.3
4.5	$8\pm2\times10^{-12}$	$2.5\pm0.8\times10^{-12}$	3.1±0.4
5	$9\pm2\times10^{-12}$	$2.5\pm0.7\times10^{-12}$	3.6±0.4
5.5	$9\pm2\times10^{-12}$	$2.8\pm0.8\times10^{-12}$	3.5±0.3
6	$1\pm3\times10^{-11}$	$3\pm1\times10^{-12}$	3.6±0.4

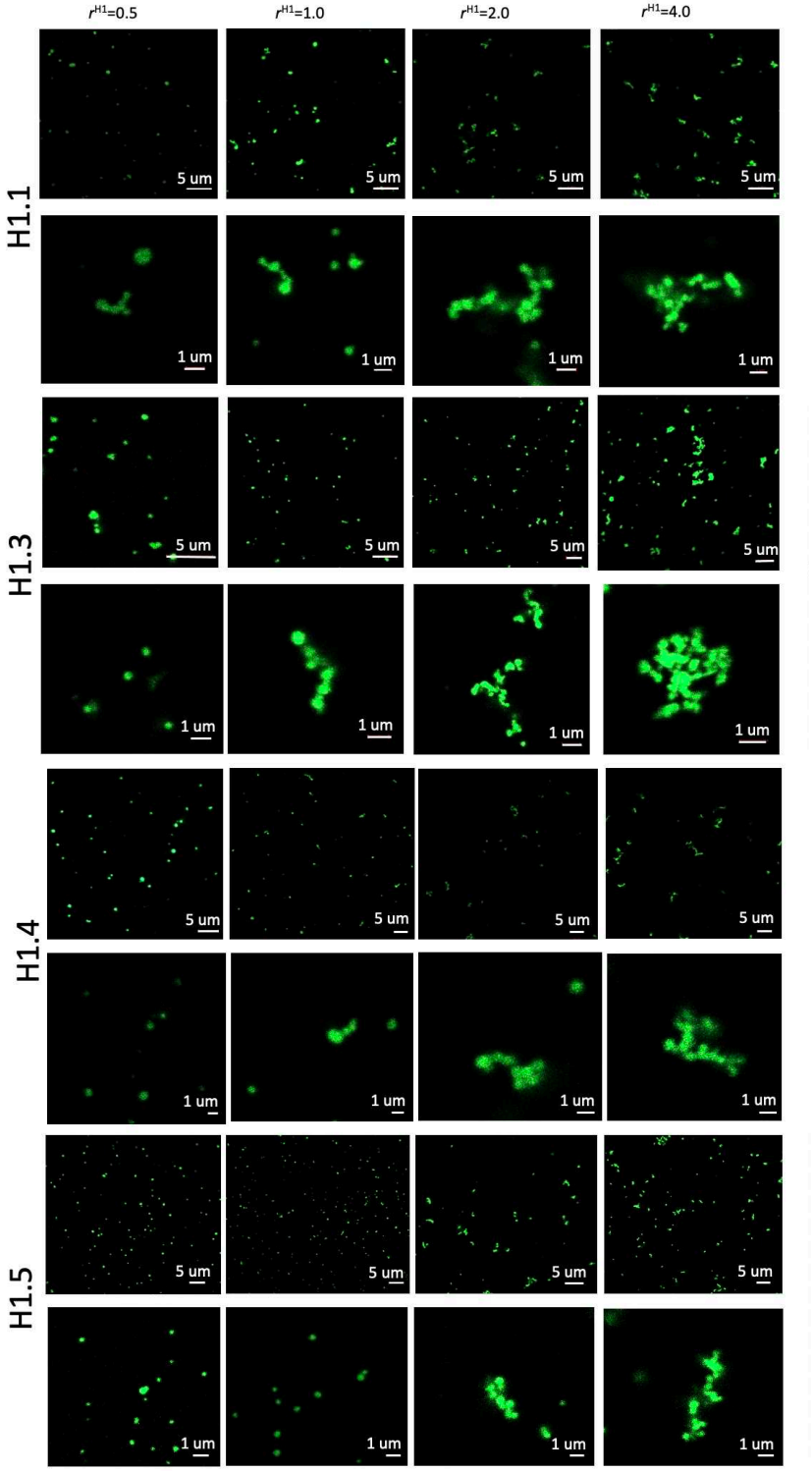

Figure 4.5: ***Linker Histones Facilitate Complex Chromatin Fiber Contacts in vitro.*** Alexa 488 labeled 601x12 condensates (5 mM Mg^{2+}) were incubated with increasing ratios (0.5, 1.0, 2.0, and 4.) of H1/N. of H1.1, H1.3, H1.4, H1.5 and visualized with fluorescence microscopy.

Chapter 5

Discussion and Future Directions

Despite more than 15 years of research and work to overturn the 30 nm folding model, it persists. In literature, it often appears in depictions of repressive H1 structures; and in introductory materials, it appears as part of the continuous folding model for chromosome formation in the nucleus (*5, 8, 36*). This may partly be due to the ease of depicting the much neater, tighter structures that 30 nm fibers appear to form. Models showing the true state of chromatin fibers as interdigitated, complex, and "messy," is much harder when introducing simplified models for students. Nevertheless, it is vital that we continue to push for more accurate portrayals of what many researchers have shown. The default state of chromatin for *Eukarya* is the complex 10 nm fiber, whether "repressive" heterochromatin domains, "open" euchromatin, or in mitotic chromosomes. This also means we need to rethink the role that linker histones play in the formation of heterochromatin, or transcriptionally repressed chromatin domains.

Chromatin condensates provide an excellent model for investigating how proteins behave in the complex 10 nm fiber environment. Condensates share many of the intrinsic properties observed in chromatin *in vivo*. They are formed by nucleosome-nucleosome interactions facilitated by the presence of divalent cations. Importantly, *in vivo* nuclei were shown to "decondense" in the absence of divalent cations, as well as when core histone tails were removed via trypsin (*57*). Condensates share the same shape and morphology of chromatin domains that have been identified through light and super resolution microscopy(*4*). They share the internal 10 nm interdigitated structure

as chromatin identified in cell nuclei. Importantly, the simplicity of their composition means that they can be tuned to a researcher's specific topic of interest. Such topics may include the effect on chromatin by changing linker DNA length, altering core histone tail domains, addition of PTMs to core histones, or the individual effects of additional chromosomal proteins. Many of these topics are difficult to study as they are involved in a variety of complex interactions in the cell nucleus. With condensates, however, we can boil down them down to very fundamental interactions using a simplified and controlled chromatin environment.

Linker histones continue to be implicated in the 30 nm folding model. However, recent evidence suggests a much more dynamic role, where linker histones act as a "liquid glue"(*40*) within chromatin. Importantly, linker histones appear to stitch together chromatin fibers, and stabilize the fiber networks. We show that higher stoichiometries of linker histones appear more efficient in the fiber cross-linking effect, as observed through fluorescent microscopy. The dynamic 10 nm fiber environment in condensates provides a more complex binding platform than is seen in the traditional 30 nm models always depicting 1:1 H1/nucleosome. Linker histones are able not only to bind individual nucleosomes, but may move within nucleosome pockets through interactions with linker DNA. These additional binding modes provide an explanation for how linker histones behave like the "glue" between chromatin fibers. This action can be seen in their resistance to nuclease digestion. It is also seen in the apparent increased structural stability provided to chromatin condensates in conditions that otherwise cause condensates to dissociate in solution. Condensates dissociate in the presence of higher levels of monovalent salts, likely through a shielding effect by the salt on DNA. BSA also

causes condensates to dissociate, possibly by preventing weak and transient nucleosome-nucleosome interactions. When linker histones are bound to condensates, they prevent BSA from causing them to apparently fall apart.

The stabilizing and cross-linking effect of linker histones may explain their role in apparent compartment maintenance. Chromatin compartments have been defined by Hi-C studies through their increased number of intradomain DNA-DNA contacts. When linker histone stoichiometries are greatly reduced, B type compartments, which are seen as “repressive,” were seen to shift to A type, which are believed to be more “open”(*52*). Therefore, compartment construction may rely on adjusting the regional density of linker histones. The high density of linker histones would serve to stabilize and increase the number of DNA-DNA contacts within a given region of chromatin. This also may contribute to a form phase separation between different functional domains within chromatin.

We also observed variant specific differences in how linker histone isoforms appeared to saturate condensates. Linker histones H1.1 and H1.2 appeared to saturate condensates at higher levels than isoforms H1.3, H1.4 and H1.5. The variations in the size and charge density of linker histones CTD may account for these observed differences. H1.1 and H1.2 have shorter C-terminal tails than H1.3, H1.4, and H1.5. The CTD of linker histones is characterized by a high density of positively charged residues. This positively charged atmosphere likely forms a stabilizing interaction with the negatively charged linker DNA. Reducing the amount of charge on the CTD may affect the apparent binding affinity of the isoforms for chromatin, making off-dyad linker histone-chromatin interactions more transient and flexible.

Finally, there is much work that can be done to follow up on the results presented here. For example, the presence of linker histones bound to di-nucleosomes appears to promote the methylation by several methyltransferases (*35*). One potential study that could be done with condensates would involve probing methyltransferase activity in condensates, both in the presence and absence of linker histones. Additionally, within the chromatin environment *in vivo*, multiple variants of linker histones are present at different concentrations. Therefore, it would be of great interest to assess the accessibility of additional proteins in the presence of multiple linker histone variants. Finally, a follow up to the apparent binding differences between variants H1.1, H1.2, H1.3, H1.4 and H1.5 would involve removal of CTD of one or more of the variants, or changes to the local charge densities on variants CTD through point mutations or tail truncations, to assess if differences we observed in binding saturation remain.

References

1. K. Luger, A. W. Mäder, R. K. Richmond, D. F. Sargent, T. J. Richmond, Crystal structure of the nucleosome core particle at 2.8 A resolution. *Nature* **389**, 251-260 (1997).
2. J. C. Hansen, K. Maeshima, M. J. Hendzel, The solid and liquid states of chromatin. *Epigenetics Chromatin* **14**, 50 (2021).
3. Z. Adhireksan *et al.*, Engineering nucleosomes for generating diverse chromatin assemblies. *Nucleic Acids Res* **49**, e52 (2021).
4. J. C. Hansen *et al.*, The 10-nm chromatin fiber and its relationship to interphase chromosome organization. *Biochem Soc Trans* **46**, 67-76 (2018).
5. D. E. Olins, A. L. Olins, Chromatin history: our view from the bridge. *Nat Rev Mol Cell Biol* **4**, 809-814 (2003).
6. P. M. Schwarz, J. C. Hansen, Formation and stability of higher order chromatin structures. Contributions of the histone octamer. *J Biol Chem* **269**, 16284-16289 (1994).
7. L. M. Carruthers, J. Bednar, C. L. Woodcock, J. C. Hansen, Linker histones stabilize the intrinsic salt-dependent folding of nucleosomal arrays: mechanistic ramifications for higher-order chromatin folding. *Biochemistry* **37**, 14776-14787 (1998).
8. D. L. Nelson, D. M. Cox, *Lehninger Principles of Biochemistry*. L. Schultz, Ed., (W. H. Freeman and Company, New York, ed. Sixth edition, 2013).
9. K. Maeshima, S. Hihara, M. Eltsov, Chromatin structure: does the 30-nm fibre exist in vivo? *Curr Opin Cell Biol* **22**, 291-297 (2010).
10. R. D. Kornberg, J. O. Thomas, Chromatin structure; oligomers of the histones. *Science* **184**, 865-868 (1974).
11. H. Kurumizaka, T. Kujirai, Y. Takizawa, Contributions of Histone Variants in Nucleosome Structure and Function. *J Mol Biol* **433**, 166678 (2021).
12. J. C. Hansen, K. E. van Holde, D. Lohr, The mechanism of nucleosome assembly onto oligomers of the sea urchin 5 S DNA positioning sequence. *J Biol Chem* **266**, 4276-4282 (1991).
13. A. A. Kalashnikova, M. E. Porter-Goff, U. M. Muthurajan, K. Luger, J. C. Hansen, The role of the nucleosome acidic patch in modulating higher order chromatin structure. *J R Soc Interface* **10**, 20121022 (2013).
14. T. Jenuwein, C. D. Allis, Translating the histone code. *Science* **293**, 1074-1080 (2001).
15. J. R. Daban, High concentration of DNA in condensed chromatin. *Biochem Cell Biol* **81**, 91-99 (2003).
16. S. A. Grigoryev, C. L. Woodcock, Chromatin organization - the 30 nm fiber. *Exp Cell Res* **318**, 1448-1455 (2012).
17. S. A. Grigoryev *et al.*, Hierarchical looping of zigzag nucleosome chains in metaphase chromosomes. *Proc Natl Acad Sci U S A* **113**, 1238-1243 (2016).

18. C. L. Woodcock, S. A. Grigoryev, R. A. Horowitz, N. Whitaker, A chromatin folding model that incorporates linker variability generates fibers resembling the native structures. *Proc Natl Acad Sci U S A* **90**, 9021-9025 (1993).
19. J. Bednar *et al.*, Nucleosomes, linker DNA, and linker histone form a unique structural motif that directs the higher-order folding and compaction of chromatin. *Proc Natl Acad Sci U S A* **95**, 14173-14178 (1998).
20. L. M. Carruthers, C. Tse, K. P. Walker, J. C. Hansen, Assembly of defined nucleosomal and chromatin arrays from pure components. *Methods Enzymol* **304**, 19-35 (1999).
21. L. M. Carruthers, V. R. Schirf, B. Demeler, J. C. Hansen, Sedimentation velocity analysis of macromolecular assemblies. *Methods Enzymol* **321**, 66-80 (2000).
22. J. Widom, A. Klug, Structure of the 300A chromatin filament: X-ray diffraction from oriented samples. *Cell* **43**, 207-213 (1985).
23. S. Bartolomé, A. Bermúdez, J. R. Daban, Internal structure of the 30 nm chromatin fiber. *J Cell Sci* **107 (Pt 11)**, 2983-2992 (1994).
24. J. R. Daban, A. Bermúdez, Interdigitated solenoid model for compact chromatin fibers. *Biochemistry* **37**, 4299-4304 (1998).
25. K. Maeshima, S. Hihara, H. Takata, New insight into the mitotic chromosome structure: irregular folding of nucleosome fibers without 30-nm chromatin structure. *Cold Spring Harb Symp Quant Biol* **75**, 439-444 (2010).
26. M. Eltsov, K. M. Maclellan, K. Maeshima, A. S. Frangakis, J. Dubochet, Analysis of cryo-electron microscopy images does not support the existence of 30-nm chromatin fibers in mitotic chromosomes in situ. *Proc Natl Acad Sci U S A* **105**, 19732-19737 (2008).
27. A. W. McDowall, J. M. Smith, J. Dubochet, Cryo-electron microscopy of vitrified chromosomes in situ. *EMBO J* **5**, 1395-1402 (1986).
28. C. Bouchet-Marquis, J. Dubochet, S. Fakan, Cryoelectron microscopy of vitrified sections: a new challenge for the analysis of functional nuclear architecture. *Histochem Cell Biol* **125**, 43-51 (2006).
29. S. Fakan, R. van Driel, The perichromatin region: a functional compartment in the nucleus that determines large-scale chromatin folding. *Semin Cell Dev Biol* **18**, 676-681 (2007).
30. J. Dubochet, N. Sartori Blanc, The cell in absence of aggregation artifacts. *Micron* **32**, 91-99 (2001).
31. E. Fussner *et al.*, Open and closed domains in the mouse genome are configured as 10-nm chromatin fibres. *EMBO Rep* **13**, 992-996 (2012).
32. C. L. Woodcock, Chromatin fibers observed in situ in frozen hydrated sections. Native fiber diameter is not correlated with nucleosome repeat length. *J Cell Biol* **125**, 11-19 (1994).
33. H. D. Ou *et al.*, ChromEMT: Visualizing 3D chromatin structure and compaction in interphase and mitotic cells. *Science* **357**, (2017).
34. M. A. Ricci, C. Manzo, M. F. García-Parajo, M. Lakadamyali, M. P. Cosma, Chromatin fibers are formed by heterogeneous groups of nucleosomes in vivo. *Cell* **160**, 1145-1158 (2015).
35. J. C. Hansen, Silencing the genome with linker histones. *Proc Natl Acad Sci U S A* **117**, 15388-15390 (2020).

36. D. V. Fyodorov, B. R. Zhou, A. I. Skoultchi, Y. Bai, Emerging roles of linker histones in regulating chromatin structure and function. *Nat Rev Mol Cell Biol* **19**, 192-206 (2018).
37. C. Pan, Y. Fan, Role of H1 linker histones in mammalian development and stem cell differentiation. *Biochim Biophys Acta* **1859**, 496-509 (2016).
38. X. Lu, J. C. Hansen, Revisiting the structure and functions of the linker histone C-terminal tail domain. *Biochem Cell Biol* **81**, 173-176 (2003).
39. J. C. Hansen, X. Lu, E. D. Ross, R. W. Woody, Intrinsic protein disorder, amino acid composition, and histone terminal domains. *J Biol Chem* **281**, 1853-1856 (2006).
40. E. B. Gibbs, R. W. Kriwacki, Linker histones as liquid-like glue for chromatin. *Proc Natl Acad Sci U S A* **115**, 11868-11870 (2018).
41. X. Lu, J. C. Hansen, Identification of specific functional subdomains within the linker histone H10 C-terminal domain. *J Biol Chem* **279**, 8701-8707 (2004).
42. A. Routh, S. Sandin, D. Rhodes, Nucleosome repeat length and linker histone stoichiometry determine chromatin fiber structure. *Proc Natl Acad Sci U S A* **105**, 8872-8877 (2008).
43. J. Bednar *et al.*, Structure and Dynamics of a 197 bp Nucleosome in Complex with Linker Histone H1. *Mol Cell* **66**, 729 (2017).
44. F. Song *et al.*, Cryo-EM study of the chromatin fiber reveals a double helix twisted by tetranucleosomal units. *Science* **344**, 376-380 (2014).
45. Z. Adhireksan, D. Sharma, P. L. Lee, C. A. Davey, Near-atomic resolution structures of interdigitated nucleosome fibres. *Nat Commun* **11**, 4747 (2020).
46. T. L. Caterino, J. J. Hayes, Structure of the H1 C-terminal domain and function in chromatin condensation. *Biochem Cell Biol* **89**, 35-44 (2011).
47. S. P. Hergeth, R. Schneider, The H1 linker histones: multifunctional proteins beyond the nucleosomal core particle. *EMBO Rep* **16**, 1439-1453 (2015).
48. J. Clausell, N. Happel, T. K. Hale, D. Doenecke, M. Beato, Histone H1 subtypes differentially modulate chromatin condensation without preventing ATP-dependent remodeling by SWI/SNF or NURF. *PLoS One* **4**, e0007243 (2009).
49. F. Catez, T. Ueda, M. Bustin, Determinants of histone H1 mobility and chromatin binding in living cells. *Nat Struct Mol Biol* **13**, 305-310 (2006).
50. A. A. Kalashnikova, R. A. Rogge, J. C. Hansen, Linker histone H1 and protein-protein interactions. *Biochim Biophys Acta* **1859**, 455-461 (2016).
51. R. Margueron, D. Reinberg, The Polycomb complex PRC2 and its mark in life. *Nature* **469**, 343-349 (2011).
52. M. A. Willcockson *et al.*, H1 histones control the epigenetic landscape by local chromatin compaction. *Nature* **589**, 293-298 (2021).
53. S. E. Healton *et al.*, H1 linker histones silence repetitive elements by promoting both histone H3K9 methylation and chromatin compaction. *Proc Natl Acad Sci U S A* **117**, 14251-14258 (2020).
54. T. Nozaki *et al.*, Condensed but liquid-like domain organization of active chromatin regions in living human cells. *Sci Adv* **9**, eadf1488 (2023).
55. C. A. Davey, D. F. Sargent, K. Luger, A. W. Maeder, T. J. Richmond, Solvent mediated interactions in the structure of the nucleosome core particle at 1.9 a resolution. *J Mol Biol* **319**, 1097-1113 (2002).

56. C. A. Davey, T. J. Richmond, DNA-dependent divalent cation binding in the nucleosome core particle. *Proc Natl Acad Sci U S A* **99**, 11169-11174 (2002).
57. P. M. Schwarz, A. Felthauser, T. M. Fletcher, J. C. Hansen, Reversible Oligonucleosome Self-Association: Dependence on Divalent Cations and

Core Histone Tail Domains. *Biochemistry* **35**, 4009-4015 (1996).
58. R. Strick, P. L. Strissel, K. Gavrilov, R. Levi-Setti, Cation-chromatin binding as shown by ion microscopy is essential for the structural integrity of chromosomes. *J Cell Biol* **155**, 899-910 (2001).
59. K. Maeshima *et al.*, Nucleosomal arrays self-assemble into supramolecular globular structures lacking 30-nm fibers. *EMBO J* **35**, 1115-1132 (2016).
60. F. Gordon, K. Luger, J. C. Hansen, The core histone N-terminal tail domains function independently and additively during salt-dependent oligomerization of nucleosomal arrays. *J Biol Chem* **280**, 33701-33706 (2005).
61. L. N. Mishra, S. Pepenella, R. Rogge, J. C. Hansen, J. J. Hayes, Acetylation Mimics Within a Single Nucleosome Alter Local DNA Accessibility In Compacted Nucleosome Arrays. *Sci Rep* **6**, 34808 (2016).
62. H. Strickfaden *et al.*, Condensed Chromatin Behaves like a Solid on the Mesoscale In Vitro and in Living Cells. *Cell* **183**, 1772-1784.e1713 (2020).
63. B. A. Gibson *et al.*, Organization of Chromatin by Intrinsic and Regulated Phase Separation. *Cell* **179**, 470-484.e421 (2019).
64. T. Nozaki *et al.*, Dynamic Organization of Chromatin Domains Revealed by Super-Resolution Live-Cell Imaging. *Mol Cell* **67**, 282-293.e287 (2017).
65. K. Maeshima, S. Ide, K. Hibino, M. Sasai, Liquid-like behavior of chromatin. *Curr Opin Genet Dev* **37**, 36-45 (2016).
66. P. T. Lowary, J. Widom, New DNA sequence rules for high affinity binding to histone octamer and sequence-directed nucleosome positioning. *J Mol Biol* **276**, 19-42 (1998).
67. K. Luger, T. J. Rechsteiner, T. J. Richmond, Preparation of nucleosome core particle from recombinant histones. *Methods Enzymol* **304**, 3-19 (1999).
68. R. A. Rogge *et al.*, Assembly of nucleosomal arrays from recombinant core histones and nucleosome positioning DNA. *J Vis Exp*, (2013).
69. J. C. Hansen, D. Lohr, Assembly and structural properties of subsaturated chromatin arrays. *J Biol Chem* **268**, 5840-5848 (1993).
70. S. M. Alonso Villela *et al.*, A protocol for recombinant protein quantification by densitometry. *Microbiologyopen* **9**, 1175-1182 (2020).
71. B. R. Zhou *et al.*, Structural Mechanisms of Nucleosome Recognition by Linker Histones. *Mol Cell* **59**, 628-638 (2015).
72. W. An, S. H. Leuba, K. van Holde, J. Zlatanova, Linker histone protects linker DNA on only one side of the core particle and in a sequence-dependent manner. *Proc Natl Acad Sci U S A* **95**, 3396-3401 (1998).
73. S. Belikov, C. Astrand, O. Wrange, Mechanism of histone H1-stimulated glucocorticoid receptor DNA binding in vivo. *Mol Cell Biol* **27**, 2398-2410 (2007).
74. L. Onn *et al.*, SIRT6 is a DNA double-strand break sensor. *Elife* **9**, (2020).
75. W. H. Liu *et al.*, Multivalent interactions drive nucleosome binding and efficient chromatin deacetylation by SIRT6. *Nat Commun* **11**, 5244 (2020).

76. Z. Yuan, R. Georgescu, G. D. Schauer, M. E. O'Donnell, H. Li, Structure of the polymerase ε holoenzyme and atomic model of the leading strand replisome. *Nat Commun* **11**, 3156 (2020).
77. P. Bouvet, S. Dimitrov, A. P. Wolffe, Specific regulation of Xenopus chromosomal 5S rRNA gene transcription in vivo by histone H1. *Genes Dev* **8**, 1147-1159 (1994).
78. A. E. White, A. R. Hieb, K. Luger, A quantitative investigation of linker histone interactions with nucleosomes and chromatin. *Sci Rep* **6**, 19122 (2016).
79. H. Yue, H. Fang, S. Wei, J. J. Hayes, T. H. Lee, Single-Molecule Studies of the Linker Histone H1 Binding to DNA and the Nucleosome. *Biochemistry* **55**, 2069-2077 (2016).
80. Y. Li *et al.*, Analysis of three-dimensional chromatin packing domains by chromatin scanning transmission electron microscopy (ChromSTEM). *Sci Rep* **12**, 12198 (2022).
81. E. Miron *et al.*, Chromatin arranges in chains of mesoscale domains with nanoscale functional topography independent of cohesin. *Sci Adv* **6**, (2020).
82. S. S. Rao *et al.*, A 3D map of the human genome at kilobase resolution reveals principles of chromatin looping. *Cell* **159**, 1665-1680 (2014).
83. B. Bintu *et al.*, Super-resolution chromatin tracing reveals domains and cooperative interactions in single cells. *Science* **362**, (2018).
84. S. W. Harshman, N. L. Young, M. R. Parthun, M. A. Freitas, H1 histones: current perspectives and challenges. *Nucleic Acids Res* **41**, 9593-9609 (2013).
85. J. P. Th'ng, R. Sung, M. Ye, M. J. Hendzel, H1 family histones in the nucleus. Control of binding and localization by the C-terminal domain. *J Biol Chem* **280**, 27809-27814 (2005).
86. C. Wood *et al.*, Post-translational modifications of the linker histone variants and their association with cell mechanisms. *FEBS J* **276**, 3685-3697 (2009).
87. T. J. Stasevich, F. Mueller, D. T. Brown, J. G. McNally, Dissecting the binding mechanism of the linker histone in live cells: an integrated FRAP analysis. *EMBO J* **29**, 1225-1234 (2010).
88. R. Wang *et al.*, Isoelectric Bovine Serum Albumin: Robust Blocking Agent for Enhanced Performance in Optical-Fiber Based DNA Sensing. *ACS Sens* **2**, 257-262 (2017).

Appendix

Additional Supporting Tables and Figures

Appendix Table 1: Mean Effective Condensate Radius (nm).

From fluorescence microscopy, condensate sizes were quantified by effective radius (longest length) in nm as a function of r^{H1}. Error shown as standard deviation.

r^{H1}	0	0.5	1	2	4
H1.0	260 ± 100	280 ± 150	460 ± 250	380 ± 170	570 ± 420
H1x		280 ± 120	290 ± 110	360 ± 160	310 ± 130
H1.1		320 ± 160	380 ± 220	390 ± 220	320 ± 130
H1.2		280 ± 120	300 ± 200	400 ± 200	440 ± 410
H1.3		300 ± 200	320 ± 170	390 ± 220	480 ± 380
H1.4		260 ± 120	330 ± 150	390 ± 250	410 ± 240
H1.5		200 ± 100	270 ± 110	380 ± 240	390 ± 290

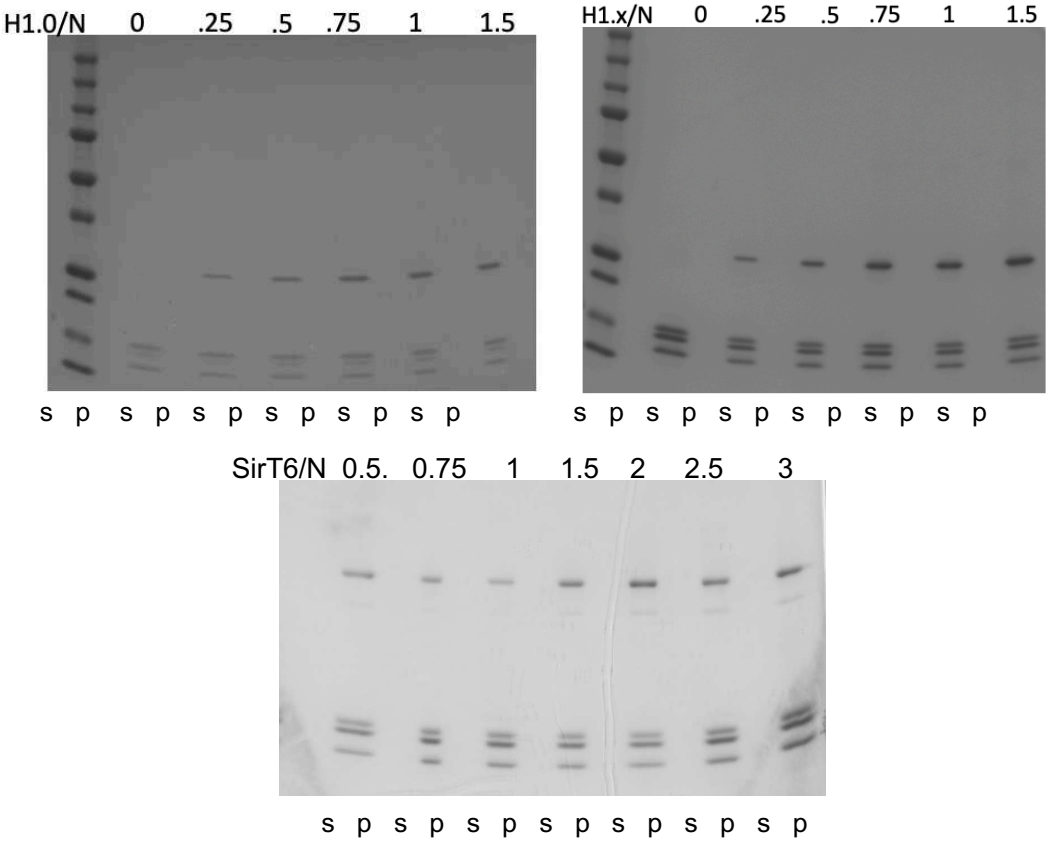

Appendix Figure 2: Biochemical Pelleting Assay with Linker Histones and SirT6. Linker histones and SirT6 incubated with condensates at increasing ratios show no detectable excess protein in the supernatant (s) fractions. Pellet fractions denoted as (p) and supernatant fractions shown as (s). Biorad Precision Plus All Blue Standards protein ladder shown for reference.

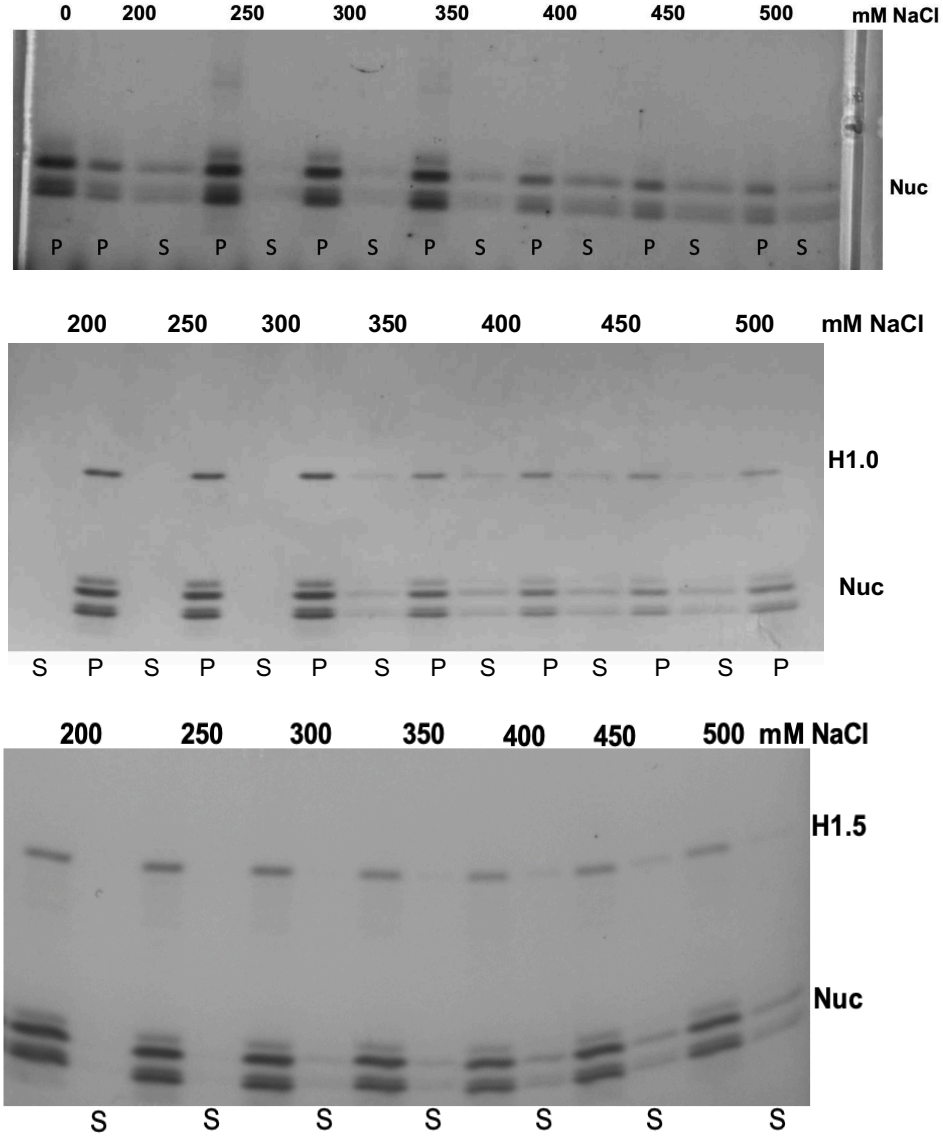

Appendix Figure 3: ***Electrostatic Interactions Between Histones and DNA Facilitate Self-Associative Properties of Condensates.*** Differential Centrifugation Pelleting Assay on 601x12 condensates over an increasing salt gradient of 200 to 500 mM NaCl shown with the addition of H1.0 and H1.5. (S) denotes supernatant fractions, (P) denotes pellet fractions. Additional shielding by monovalent-cationic species in solution prevents nucleosomes from binding DNA. Titrating in higher amounts of salt to condensates show that nucleosomes become unbound by 200 mM NaCl. The addition of linker histones H1.0 and H1.5 show that nucleosomes remain bound to DNA within condensates up to 350 mM NaCl. This indicates the stabilization effect of linker histones observed here is electrostatic in nature.

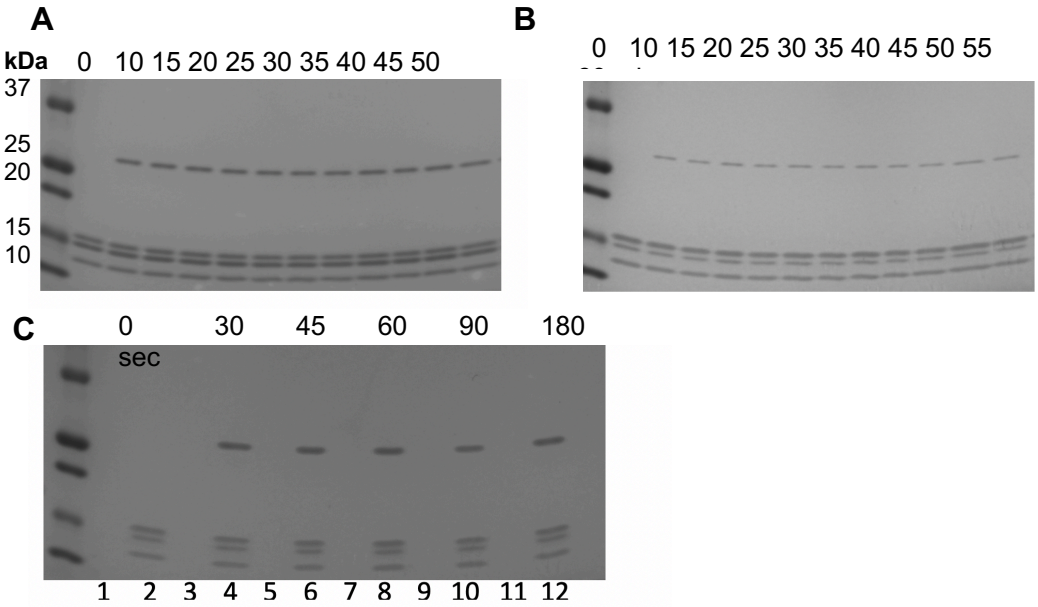

Appendix Figure 4: ***Linker Histones Display Rapid Binding to Condensates.*** **A:** H1.0 was mixed with pre-formed condensates at 25 C for the given time in minutes before pelleting. Only pellets were analyzed using SDS-PAGE. **B:** H1x was mixed with pre-formed condensates at 25 C for the given time points in minutes. Only pellets were analyzed. **C:** H1x was mixed with pre-formed condensates at 4 C for given time-points in seconds. Even lanes represent pellets, odd lanes represent supernatant. Biorad Precision Plus All Blue Standards protein ladder shown for reference.

Linker Histones Display Rapid Binding to Condensates

The binding rate of linker histones to the 208 bp condensate is unknown, and may show variation among the different linker histone isoforms. We attempted to determine the rate of binding using the biochemical pelleting assay. First, we incubated 2:1 H1.0 to nucleosome at different time points, starting at 10 minutes, and checking every 5 minutes up to 1 hour at 25 C. In figure A4A, we see that by 10 minutes, through 60 minutes, H1.0 appears to be bound to the condensates. Similarly, as shown in figure A4B, the same experiment was repeated with H1x. H1x also showed apparent binding within the first 10 minutes of its introduction. Supernatant fractions were run on separate gels and showed no detectable amounts of either H1.0 or H1x. Therefore, we repeated the experiment using H1x at 4 C, and reduced the time points to 30 second intervals up to 180 seconds. As shown in figure A4C, H1x appears to show complete binding within 30 seconds, with no detectable amounts of H1x in the supernatant. Even at reduced temperature, H1x displays a rapid and complete binding under 1 minute. The sensitivity limits of this assay therefore preclude us from using it to make any kinetic measurements. However, it is important to note that apparent binding of H1 to condensates is rapid, even under conditions of low temperature.

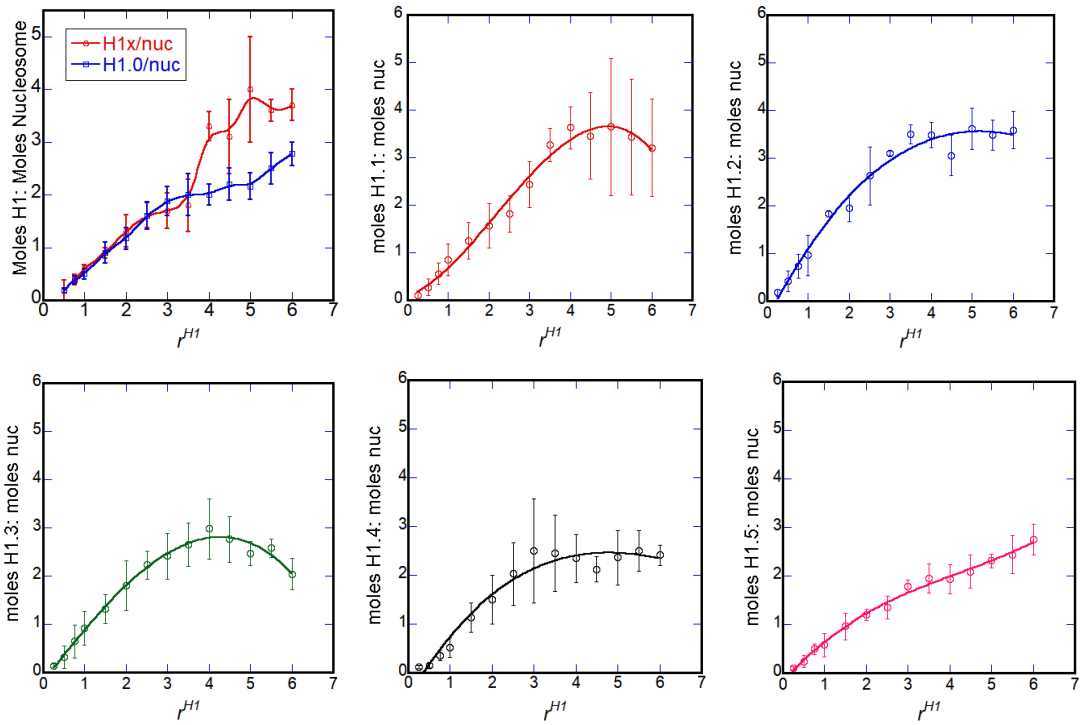

Appendix Figure 5: Additional Binding Plots for Human Somatic Linker Histone Isoforms. Binding plots for linker histones were generated by analyzing mole ratios of linker histone to core histones in the pellet fraction from the biochemical pelleting assay. The horizontal axis represents the input mole ratio of linker histone per nucleosome. The vertical axis represents the measured amount of H1 per nucleosome (H1/N) found in the pellet fractions. Band intensities were measured using ImageJ, and converted to ug H1 using in-gel standards and a standard plot.

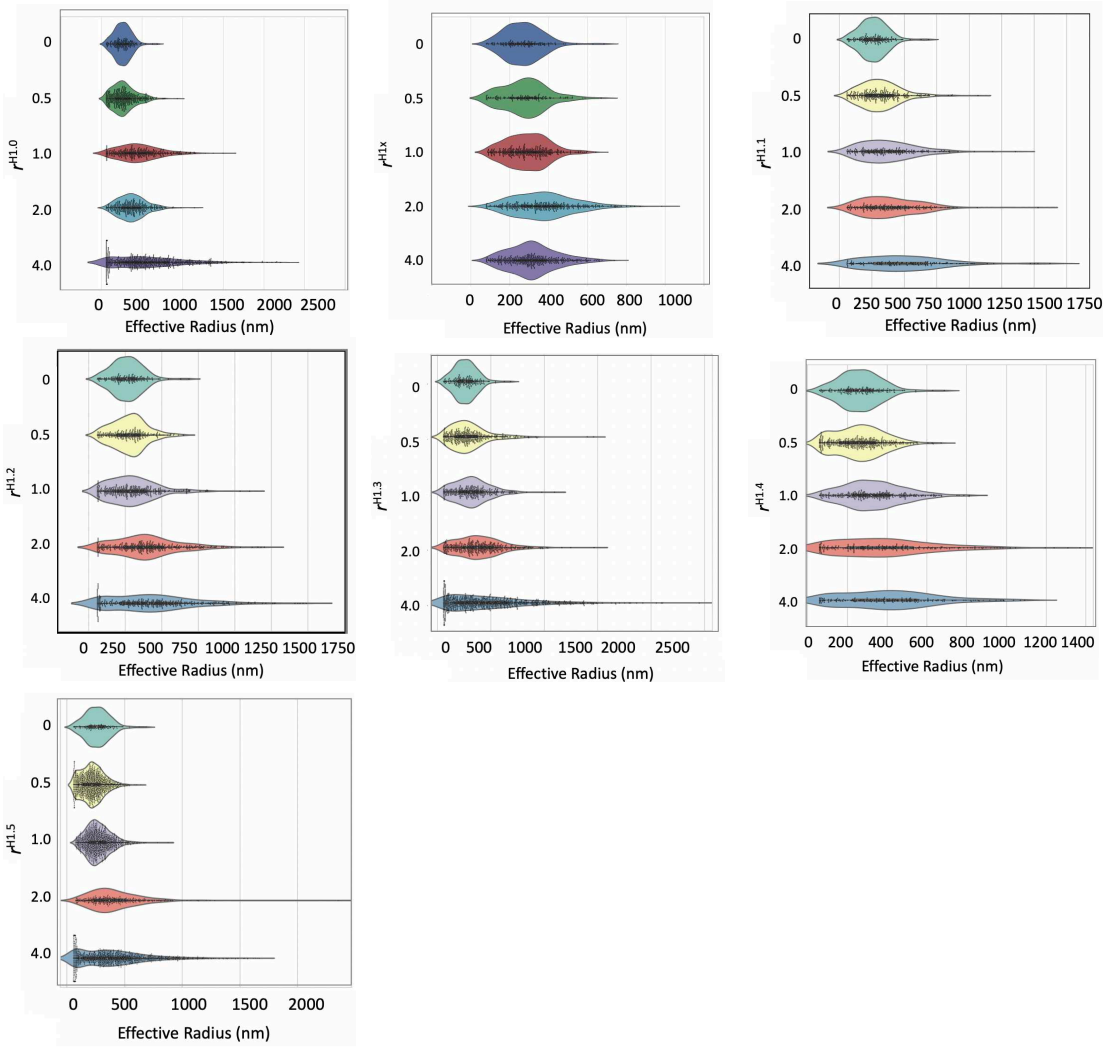

Appendix Figure 6: Distribution of Condensate Radius by r^{H1} for Human Somatic Linker Histone Variants. Violin plots calculated from fluorescent microscopy images on condensates quantitated in bulk using matplotlib.pyplot, python code developed by Gabriel Galindo at Colorado State University. Condensate radii were measured by drawing a rectangle around continuous chains or aggregates and treating the area as a "segmented coin."

TATCGGACCCTATACGCGGCCGCCCTGGAGAATCCCGGTGCCGAGGCCGCTCAATTGGTCGTAGAC
AGCTCTAGCACCGCTTAAACGCACGTACGCGCTGTCCCCCGCGTTTTAACCGCCAAGGGGATTACTC
CCTAGTCTCCAGGCACGTGTCAGATATATACATCCTGTGCATGTGGATCCGAATTCATATTAATTAATA
CTAGATATCGGACCCTATACGCGGCCGCCCTGGAGAATCCCGGTGCCGAGGCCGCTCAATTGGTCG
TAGACAGCTCTAGCACCGCTTAAACGCACGTACGCGCTGTCCCCCGCGTTTTAACCGCCAAGGGGA
TTACTCCCTAGTCTCCAGGCACGTGTCAGATATATACATCCTGTGCATGTGGATCCGAATTCATATTA
ATTAATACTAGATATCGGACCCTATACGCGGCCGCCCTGGAGAATCCCGGTGCCGAGGCCGCTCAA
TTGGTCGTAGACAGCTCTAGCACCGCTTAAACGCACGTACGCGCTGTCCCCCGCGTTTTAACCGCCA
AGGGGATTACTCCCTAGTCTCCAGGCACGTGTCAGATATATACATCCTGTGCATGTGGATCCGAATT
CATATTAATTAATACTAGATATCGGACCCTATACGCGGCCGCCCTGGAGAATCCCGGTGCCGAGGCC
GCTCAATTGGTCGTAGACAGCTCTAGCACCGCTTAAACGCACGTACGCGCTGTCCCCCGCGTTTTAA
CCGCCAAGGGGATTACTCCCTAGTCTCCAGGCACGTGTCAGATATATACATCCTGTGCATGTGGATC
CGAATTCATATTAATTAATACTAGATATCGGACCCTATACGCGGCCGCCCTGGAGAATCCCGGTGCC
GAGGCCGCTCAATTGGTCGTAGACAGCTCTAGCACCGCTTAAACGCACGTACGCGCTGTCCCCCGC
GTTTTAACCGCCAAGGGGATTACTCCCTAGTCTCCAGGCACGTGTCAGATATATACATCCTGTGCATG
TGGATCCGAATTCATATTAATTAATACTAGATATCGGACCCTATACGCGGCCGCCCTGGAGAATCCCG
GTGCCGAGGCCGCTCAATTGGTCGTAGACAGCTCTAGCACCGCTTAAACGCACGTACGCGCTGTCC
CCCGCGTTTTAACCGCCAAGGGGATTACTCCCTAGTCTCCAGGCACGTGTCAGATATATACATCCTG
TGCATGTGGATCCGAATTCATATTAATTAATACTAGATATCGGACCCTATACGCGGCCGCCCTGGAGA
ATCCCGGTGCCGAGGCCGCTCAATTGGTCGTAGACAGCTCTAGCACCGCTTAAACGCACGTACGCG
CTGTCCCCCGCGTTTTAACCGCCAAGGGGATTACTCCCTAGTCTCCAGGCACGTGTCAGATATATAC
ATCCTGTGCATGTGGATCCGAATTCATATTAATTAATACTAGATATCGGACCCTATACGCGGCCGCCC
TGGAGAATCCCGGTGCCGAGGCCGCTCAATTGGTCGTAGACAGCTCTAGCACCGCTTAAACGCACG
TACGCGCTGTCCCCCGCGTTTTAACCGCCAAGGGGATTACTCCCTAGTCTCCAGGCACGTGTCAGAT
ATATACATCCTGTGCATGTGGATCCGAATTCATATTAATTAATACTAGATATCGGACCCTATACGCGG
CCGCCCTGGAGAATCCCGGTGCCGAGGCCGCTCAATTGGTCGTAGACAGCTCTAGCACCGCTTAAA
CGCACGTACGCGCTGTCCCCCGCGTTTTAACCGCCAAGGGGATTACTCCCTAGTCTCCAGGCACGT
GTCAGATATATACATCCTGTGCATGTGGATCCGAATTCATATTAATTAATACTAGATATCGGACCCTAT
ACGCGGCCGCCCTGGAGAATCCCGGTGCCGAGGCCGCTCAATTGGTCGTAGACAGCTCTAGCACC
GCTTAAACGCACGTACGCGCTGTCCCCCGCGTTTTAACCGCCAAGGGGATTACTCCCTAGTCTCCAG
GCACGTGTCAGATATATACATCCTGTGCATGTGGATCCGAATTCATATTAATTAATACTAGATATCGGA
CCCTATACGCGGCCGCCCTGGAGAATCCCGGTGCCGAGGCCGCTCAATTGGTCGTAGACAGCTCTA
GCACCGCTTAAACGCACGTACGCGCTGTCCCCCGCGTTTTAACCGCCAAGGGGATTACTCCCTAGTC
TCCAGGCACGTGTCAGATATATACATCCTGTGCATGTGGATCCGAATTCATATTAATTAATACTAGATA
TCGGACCCTATACGCGGCCGCCCTGGAGAATCCCGGTGCCGAGGCCGCTCAATTGGTCGTAGACAG
CTCTAGCACCGCTTAAACGCACGTACGCGCTGTCCCCCGCGTTTTAACCGCCAAGGGGATTACTCCC
TAGTCTCCAGGCACGTGTCAGATATATACATCCTGTGCATGTGGATCCGAATTCA

Sequence of each Repeat, Widom 601 Positioning Sequence Highlighted in Red:

TAGATATCGGACCCTATACGCGGCCGCCCTGGAGAATCCCGGTGCCGAGGCCGCTCAATTGGTCGT
AGACAGCTCTAGCACCGCTTAAACGCACGTACGCGCTGTCCCCCGCGTTTTAACCGCCAAGGGGAT
TACTCCCTAGTCTCCAGGCACGTGTCAGATATATACATCCTGTGCATGTGGATCCGAATTCATATTAA
TTAATAC

Appendix Figure 7: Full DNA Sequence of 2467 bp 601X12 Insert. Shown below, the sequence of each individual repeat is shown, with the 144 bp 601 positioning sequence highlighted in red. Each repeat is 207 bp total.